FILTERED RAYLEIGH SCATTERING MEASUREMENTS IN A BUOYANT FLOWFIELD

THESIS

Christopher C. McGaha, Captain, USAF

AFIT/GAE/ENY/07-M18

DEPARTMENT OF THE AIR FORCE
AIR UNIVERSITY

AIR FORCE INSTITUTE OF TECHNOLOGY

Wright-Patterson Air Force Base, Ohio

The views expressed in this thesis are those of the author and do not reflect the official policy or position of the United States Air Force, Department of Defense, or the U.S. Government.

AFIT/GAE/ENY/07-M18

FILTERED RAYLEIGH SCATTERING MEASURMENTS IN A BUOYANT FLOWFIELD

THESIS

Presented to the Faculty

Department of Aeronautical Engineering

Graduate School of Engineering and Management

Air Force Institute of Technology

Air University

Air Education and Training Command

In Partial Fulfillment of the Requirements for the

Degree of Master of Science in Engineering

Christopher C. McGaha, BSME

Captain, USAF

March 2007

AFIT/GAE/ENY/07-M18

FILTERED RAYLEIGH SCATTERING MEASURMENTS IN A BUOYANT FLOWFIELD

Christopher C. McGaha, BSME

Captain, USAF

Approved:

/SIGNED/	15 Mar 2007
Mark F. Reeder, Professor (Chairman)	Date
/SIGNED/	15 Mar 2007
Paul I. King, Professor (Member)	Date
/SIGNED/	15 Mar 2007
Richard D. Branam, Major, USAF (Member)	Date

Acknowledgments

I would like to express my sincere appreciation to my faculty advisor, Professor Mark Reeder, for his guidance and support throughout the course of this thesis effort. His insight and experience was critical to my understanding of the subject and his encouragement was certainly appreciated. I would also like to thank the technicians, Barry Page and Chris Zickerfoose, whose help setting up and maintaining the experiment was appreciated.

Christopher C. McGaha

.

Table of Contents

Page

List of Figures

Page

List of Tables

Page

Nomenclature

BG…….Background power in image

E_0……Intensity of irradiating light source

FRS……Filtered Rayleigh scattering

I……Scattered power

σ…….Rayleigh scattering cross section

X……Mole fraction concentration

Abstract

Filtered Rayleigh Scattering (FRS) is a non-intrusive technique for studying flowfields. It utilizes a narrow linewidth laser, an absorption filter, and a detector. Molecular scattering provides the signal to the camera, and the difference in molecular cross section can be used to discriminate between unmixed gaseous components. The focus of this research is to document the behavior of a horizontal buoyant jet using FRS. A helium jet of precisely controlled mass flow rate is injected into a standard room temperature environment, and FRS provides the means to measure its core trajectory and mixing rate. Trajectory analysis, conducted with consideration of the Reynolds number and Grashof number, can be used to compare these results to the literature. A significant portion of the study was dedicated to measuring the rate at which FRS data can be acquired with a continuous wave laser. Additionally, mixing patterns for the buoyant jet were collected and indicate that core low-density fluid is expelled into the ambient region in a striking manner under certain conditions. Although such an expulsion of core low-density fluid has been noted in the literature, it has generally been associated only with an upward direction. This was observed at a Reynolds number of 238. However, at a Reynolds number of 667, the jet appears to take on features of jets subjected to an exaggerated form of helical mode excitation. The physics behind this phenomena requires additional study.

FILTERED RAYLEIGH SCATTERING MEASUREMENTS IN A BUOYANT FLOWFIED

I. Introduction

Background

Traditional techniques for measuring data in a flowfield include, but are not limited to, the use of hotwire anemometry, thermocouples, and pitot tubes. These techniques require the placement of physical devices in the flowfield, thus affecting the physics of the flow regime. These devices are also limited to collecting data at only one location within the flowfield at a single instant in time. An improved solution is to collect flowfield data without inserting any physical devices in the flowfield while also simultaneously capturing data at multiple locations throughout the flowfield. Filtered Rayleigh scattering (FRS), a laser based flow diagnostics technique and introduced in 1990 (Miles and Lempert, 1990), is the right solution for the task at hand.

Filtered Rayleigh scattering is a non-intrusive method used to measure the flow characteristics of a flowfield such as species concentration, temperature, velocity, and density. The Rayleigh scattering signal provides this thermodynamic data and FRS can also be used to generate useful flow visualizations in a flowfield. Its primary advantage over the traditional methods of collecting data in a flowfield, such as the pitot tube, hotwire anemometry, and the thermocouple, is that the flowfield is not disturbed by a probe while taking measurements. Another advantage of FRS is any light scattered off stationary surfaces in the background of an image can be nearly eliminated. Thus, the

noise to signal ratio is reduced over Rayleigh scattering based measurements which do not utilize a filter. FRS is continuing to spread throughout research facilities.

The application of FRS uses a narrow-linewidth laser, an absorption filter, and a collection device such as a camera. The laser provides a concentrated electromagnetic wave, light, across the flowfield. The absorption filter is designed to block light at different frequencies. The intensity of the light is captured by the collection device. The idea is to tune the laser at a frequency such that the light is blocked in the absence of particle motion. In the absence of particle motion, light scatters off of particles at the same frequency as the laser. Because of the thermal energy associated with the motion of particles in a quiescent environment, or the kinetic energy associated by a continuum gas flow, the frequency the light is scattered off of the gas particles is broadened into a spectra including a range of frequencies due to the Doppler effect. This broadening in the spectra allows a portion of the particle scattering to pass through the filter and this light is then collected by the camera.

Rayleigh scattering is the molecular scattering of light off of gas particles. The amount of light scattered varies directly as the square of the particle volume and inversely as the fourth power of the irradiating wavelength (McCartney, 1976). The scattering happens due to the protons and electrons associated within the atom. When a particle encounters an electromagnetic wave, the charges separate and create an oscillating dipole moment. This dipole moment generates a secondary wave at the same frequency as the incoming wave. The generation of this secondary wave is known as scattering. Rayleigh scattering applies to small particles in which the particle diameter is less than 1/10 of the

irradiating wavelength (McCartney, 1976). As the particle size is increased, the scattering is termed Mie scattering. Air and helium particles are on the order of 10^{-4} μm and are thus susceptible to Rayleigh scattering when the incoming wavelength is between 400-700 nm. Rayleigh scattering is non-intrusive because it relies on molecular scattering.

The study of bouyant jets is a widely researched field in the engineering community. Environmentalists are studying the transport of pollutants in a body of water (Law et al., 2003). The mixing characteristics of buoyant jet flames are fundamentally important to combustion researchers for improving combustion efficiency (Jiang and Luo, 2003). The engineers who maintain solar ponds need to know the exact trajectory of a brine solution in the pond so the brine is injected at the correct location (Arakeri et al., 2000). Aerodynamicists encounter buoyant jets while studying the mixing behavior of two different fluids and must appropriately account for the density difference between the fluids.

Problem Statement

This research is a continuation of the previous research effort at AFIT aimed at evaluating a FRS system. The previous research included setting up the system and was used to generate flow visualizations, capturing qualitative data. The next step towards evaluating the FRS system is to collect quantitative data. Species concentration data is a relatively easy quantity to collect using FRS and is the focused measurement of this research.

A vertical jet is a jet that is discharged in the same direction as the gravitational field. A horizontal jet is discharged perpendicular to the gravitational field. The amount of literature available for the studying of a vertical buoyant jet exceeds the available literature for the studying of a horizontal buoyant jet. Furthermore, the measurement techniques used to track jet trajectory are typically either intrusive, pointwise-based, or both. Horizontal buoyant jets are found in the combustion chamber of axial engines and in the application of maintaining solar ponds.

Research Objectives/Questions

The primary objectives of this research are to collect a single property measurement, helium concentration, in a flowfield using a FRS system and to study the behavior of a horizontal buoyant jet. Secondary objectives involve maximizing the data acquisition rate of the FRS system and expanding the physical properties collected with the FRS system, albeit in different flowfields.

Research Focus

The focus of this research is the utilization of a Filtered Rayleigh Scattering system using a continuous argon ion laser as the illuminating source. This entails collecting FRS data at a maximum sampling rate while keeping the camera noise to FRS signal ratio at a minimum. Procedures must also be taken to ensure the flowfield is free from any unwanted particles that would potentially induce Mie scattering and dominate the Rayleigh scattering signal.

This research uses FRS to study the mixing characteristics and behavior of two different density gases in the form of a horizontal buoyant jet via species concentration measurements. The buoyant jet is generated by exhausting the less dense fluid into the more dense fluid.

Methodology

The methodology entails setting up and executing two different experiments and image processing the data. One experiment implements the concentrated laser beam and a camera to record the data from an overhead view. The other experiment required the beam be spread into a laser sheet and a camera to record the cross sectional data of the jet. A detailed description of the methodology is laid out in Chapter III of this report.

Assumptions/Limitations

The absorption filter is characterized by varying the laser etalon temperature while monitoring the laser power through the filter. An additional check at the etalon temperature setting thought to correlate with an absorption notch can be verified visually by monitoring the fluorescence of the filter. For the experiments in this research, the laser is operated at a frequency corresponding to an absorption notch of the filter, thus reducing background scattering. The filtered images are compared to unfiltered images and the effectiveness of the filter is observed.

Implications

This research further develops the utilization of the FRS system at AFIT. The necessary procedures for system operation such as characterizing the filter and measuring

the frequency of the camera are laid out for future researchers. The quantitative measurements of species concentration are a stepping stone towards collecting other properties in a flowfield. Future research of this system would eventually lead to collecting velocity and helium concentration measurements in a supersonic wind tunnel. Also, the behavior of the horizontal buoyant jet observed from this research is captivating and opens the door for additional research in this fundamental area of research.

II. Literature Review

Chapter Overview

A basic understanding of two areas of research must be gained to put the current work in its proper context. First, an in-depth explanation of the theory behind Filtered Rayleigh Scattering and the experimental setup required for execution are presented. Second, literature which documents the behavior and underlying physics of horizontal buoyant jets is described.

Rayleigh Scattering

Rayleigh scattering is the molecular scattering of incident light as shown in Figure 1 and was derived in 1871 by Lord Rayleigh (McCartney, 1976). His research provides the explanation of the blue color in the sky and can be used as a powerful diagnostic tool in fluid dynamics. Only two sources are needed for Rayleigh scattering: light and a molecule less than one -tenth of the light's wavelength. Due to the proliferation of lasers, a controlled light source is readily available and thus Rayleigh scattering techniques are becoming more attractive to researchers.

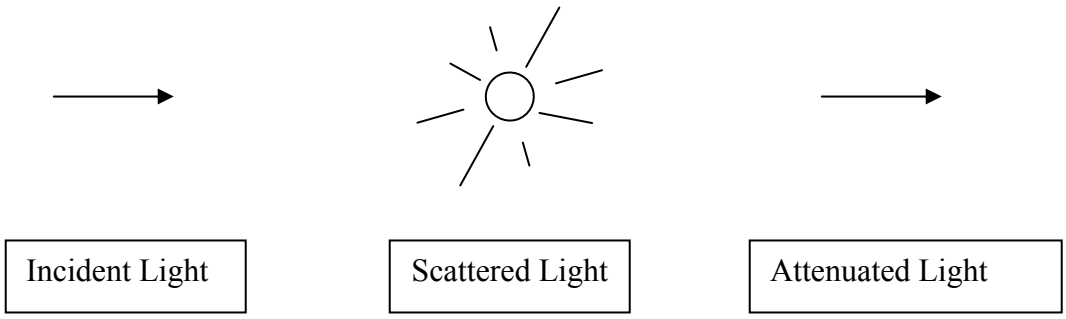

Figure 1. The light is attenuated due to the scattering

In Rayleigh scattering, a molecule can be modeled in a simplified way as a hard sphere, containing a positive charge at its nucleus with a corresponding cloud of negative charge surrounding its nucleus as shown in Figure 2. It is assumed the net force acting at the center is zero and the cloud of negative charge is uniformly distributed around the nucleus and may be treated as if it were at the center of the model. The model is assumed isotropic, linear and lightly damped. As an electromagnetic field passes through the molecule, its charges at the center are forced apart, creating an electric dipole moment. The resulting dipole moment produces a secondary electromagnetic field, causing scattering of the incident light (McCartney, 1976). The power of the secondary wave is a function of the molecular Rayleigh scattering cross section and is defined by

$$I = \sigma E_0$$

where σ is the cross section and E_0 is the intensity of the incoming wave. The two gases in this research are helium and air. The Rayleigh scattering cross section ratio of helium to air is 1.4 percent (Lee, et al., 2003).

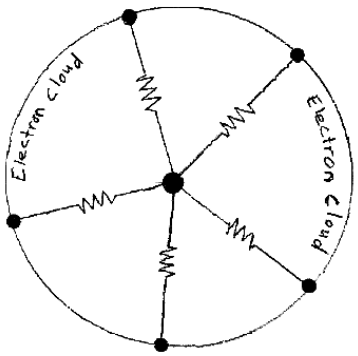

Figure 2. A hard sphere model of a molecule in molecular scattering.

Filtered Rayleigh Scattering

A laser and an absorption filter define FRS. The laser provides the light and the filter enhances the collected Rayleigh scattering signal. This is termed filtered Rayleigh scattering. The most utilized combination of a laser and absorption filter is the use of an Nd: YAG pulsed laser and an iodine filter (Boguszko and Elliot, 2005). This combination is attractive to researchers due to the absorption profiles of iodine correlating with a 532 nm wavelength (Boguszko et al., 2006, Miles et al., 2001, Boguszko et al., 2002, Boguszko and Elliot, 2005). Nd: YAG lasers produce wavelengths within the vicinity of 532 nm. However, the data collection rate using a pulsed laser is limited to the rate at which the laser pulses. The argon-ion lasers with an etalon optic are continuous and have a narrow linewidth, making this type of laser attractive to researchers aiming to improve the collection rate. Iodine absorption lines cover a broad range of wavelengths and are also accessible using argon-ion lasers (Boguszko and Elliot, 2005).

The filters used in FRS measurements are designed to transmit and block light at different wavelengths. The filters are cylindrical in shape, contain a selective gas enclosed by glass cells, and are referred to as atomic or molecular absorption filters in the literature. There are several advantages for using atomic/molecular filters in lieu of optics filters which use interferometers or spectrometers to transmit and block light at certain wavelengths. The greatest advantage is its ability to collect data over a large area without sacrificing the resolution of the transmission and blocking regions (Miles et al., 2006). This is due to the fact that the transmission and blocking regions of the filter are a

function of the absorption properties of the gas and do not rely on a narrow slit, unlike spectrometers, to transmit and block light. Another advantage is that generally, the extinction regions of an atomic or molecular filter far exceeds that of an interferometer filter and spectrometer (Miles et al., 2001).

Miles et al., 2006, investigated various gaseous candidates for use in these filters and suggested that the prime candidates for these filters are iodine vapor and mercury due to the high vapor pressure of each gas, allowing the filter to be operated only slightly above room temperature (Miles et al., 2006). As noted earlier, iodine is the most common filter used in FRS applications. Iodine is more attractive than mercury to use in a filter due to its broader range of blocking and transmission regions.

The desirable characteristics of these filters are to have steep cut-on and cut-off edges at which the light is transmitted and eliminated through the filter, have a powerful extinction of light in the blocking region and a 100% transmission in the transmission region, and block wavelengths corresponding with the available lasers. The effect of an idealized absorption filter is depicted by Miles et al., 2001, shown in Figure 3, and describes what is known as Filtered Rayleigh Scattering.

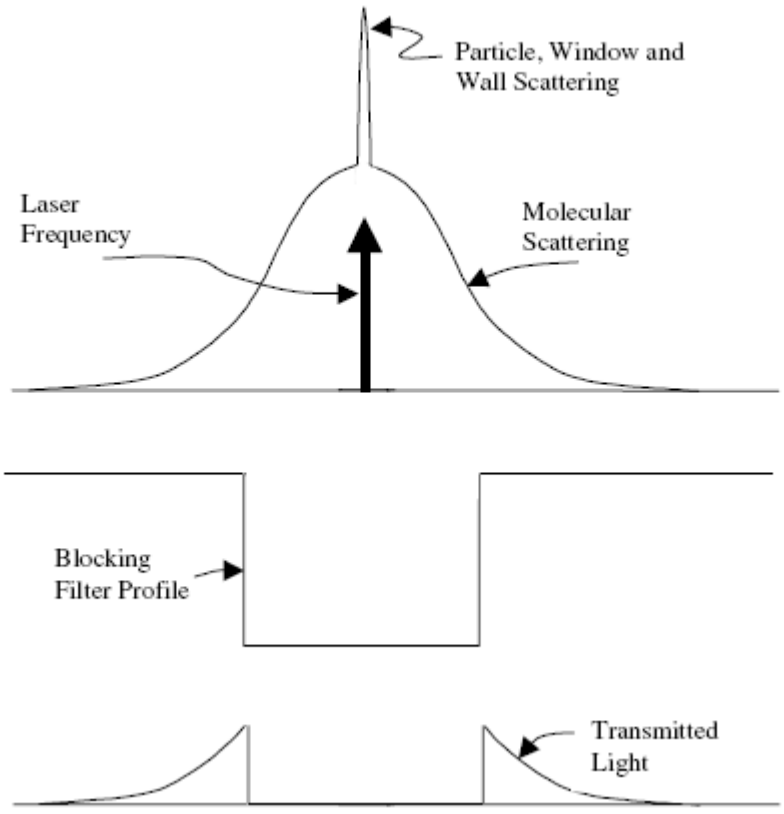

Figure 3. The effect of using a filter to remove unwanted wavelengths. (Miles et al., 2001)

Iodine has many transmissions throughout the visible spectrum and thus is an attractive selection to use in absorption filters. Iodine also has sharp cut off distinctions between the transmitted and untransmitted zones and is one of the common species found in absorption filters. Seasholtz and Buggele, 1997, calculated the iodine absorption profile using Forkey's code and their results are shown in Figure 4. The sharp cut off edges, the strong untransmitted zone, and high number of transmission zones are clearly evident.

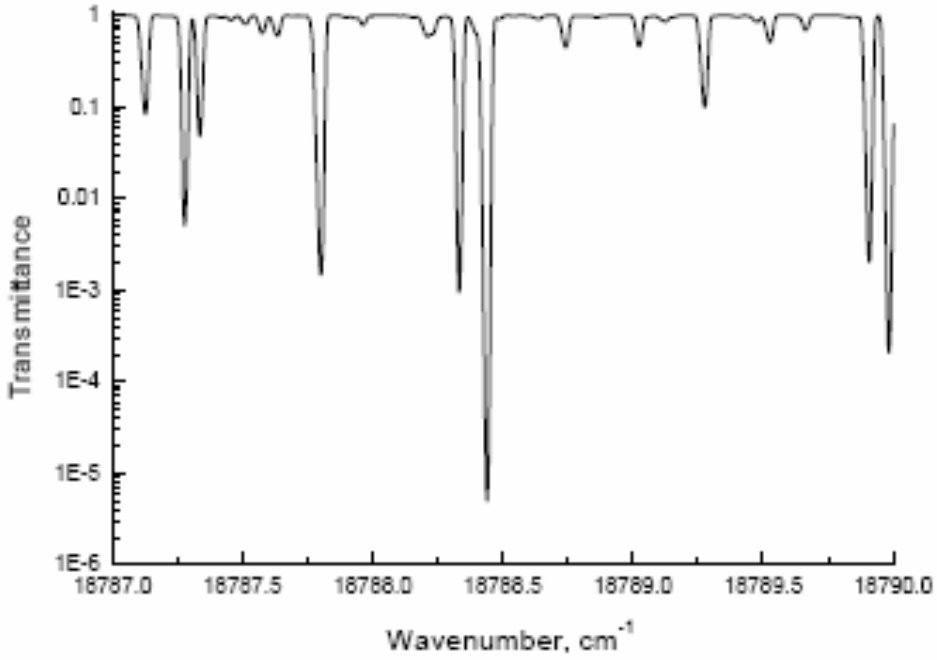

Figure 4. The calculated iodine filter profile using Forkey's code. The sharp cut off edges and strong transmission regions are clear, making iodine an attractive gas for absorption filters. The wavenumbers correlate with wavelengths in the vicinity of 532 nm. (Seasholtz and Buggele, 1997)

The Collection Device

The collection device, or detector, can be the limiting factor at which the data is collected depending on laser type in the FRS system. The objective is to capture data at the fastest sampling rate possible while keeping the additive noise to signal ratio at a minimum.

Non-Buoyant and Helical Jets

To better understand buoyant jets, non-buoyant jets are first discussed to provide an understanding of typical jet behavior. A typical jet is shown in Figure 5. As the jet is

exhausted, the jet begins to spread and entrains the outer fluid into the jet. The jet spreading increases as the jet travels further downstream (White, 2006). The mixing rate at which the jet entrains the outer fluid is of primary interest to researchers aiming to improve combustion efficiency. This region of mixing between the jet and the outer fluid is termed the mixing region of the jet. There are fluctuations associated with the mixing region of jets. For example, the species concentration fractions within the mixing region of a jet have been observed to vary with time on the order of 0 – 20 percent (Borg et al., 2001). A typical standard deviation plot of a jet will reveal the mixing and core regions of the jet. The mixing region will correlate with higher standard deviation values while the core region will correlate with lower standard deviation values. Standard deviation plots of jets are found in the cited literature of Helmer et al., 2007, and Borg et al., 2001.

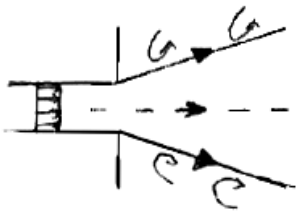

Figure 5. A typical jet spreads as it traverses downstream while entraining the ambient fluid.

An interesting type of jet, although not discussed in classical fluid textbooks such as those by White, 2006, or Bernard and Wallace, 2002, is the helical jet. Helical jets are spiral in nature and display unique features along its cross section. The jet cross section

takes on the form of a starfish pattern having five to nine azimuthal fingers (Chao et al., 2000). This unique behavior is due to the instabilities associated with helical jets. These instabilities are a direct result of the three dimensional helical jet vortices and are obviously much more difficult to analyze than those of the two dimensional modeled typical jet.

Horizontal and Vertical Buoyant Jets

A horizontal buoyant jet is a jet with the inertial forces perpendicular to the gravitational field as shown in Figure 6. The behavior from a horizontal buoyant jet is not as well documented as the behavior of a vertical buoyant jet. Horizontal buoyant jets are in the combustion chamber of a turbine and pulse detonating engine, the transport of pollutants, and in solar ponds. The most common example of a horizontal and vertical buoyant jet seen everyday is from automobile emissions and smokestacks, respectively.

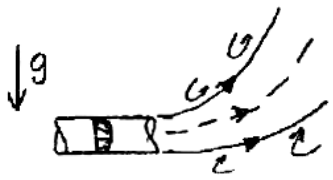

Figure 6. A horizontal buoyant jet will generally have an upward motion associated with the jet.

Buoyant jets are characterized by their inertial and buoyancy forces in the form of non-dimensional numbers. The inertial forces are described by the Reynolds number while the buoyancy forces are described in the referenced literature by alternatively, the

Grashof, Froude, or Richardson number depending on the author. The Reynolds, Grahsof, Froude, and Richardson numbers are defined in equation (1).

$$\begin{aligned} \mathrm{Re} &= \frac{\rho V d}{\mu} \\ Gr &= \frac{g(\rho_a - \rho_j)d^3}{\mu^2 / \rho_j} \\ Fr &= \mathrm{Re}/\, Gr^{1/2} \\ Ri &= Gr / \mathrm{Re}^2 \end{aligned} \tag{1}$$

These non-dimensional numbers characterize the flow regime of the jet. White, 2006, uses the Grashof and Reynolds numbers to describe the jet regime by either forced, free, or mixed convection. Forced convection dominates the jet regime when the Grashof number is much less (<<) than the Reynolds number squared. Free convection dominates the jet regime when the Grahsof number is much greater (>>) than the Reynolds number squared. Both forced and free convection are important in the jet regime when the Grashof number is on the order of the Reynolds number squared.

Both laminar and turbulent buoyant jets are explored in the literature. The methods used to study the buoyant jets are predominately experimental including laser imaging, shadowgraph photography, and the use of thermocouples in an isothermal medium. Similar to non-buoyant jets, the mixing rate characteristics and jet spread are fundamentally important to the study of buoyant jets. However, in the case of studying horizontal buoyant jets, an additional parameter is added, namely the jet trajectory.

The trajectory and mixing behavior of a laminar horizontal buoyant jet are unique. The jet will bifurcate under different operating conditions as shown in Figure 1 of the referenced work by Arakeri et al., 2000.

> "Bifurcation is related to the fact that velocity varies across any cross section of the jet. For a given density difference, fluid particles having higher velocity will have flatter trajectory than those having lower velocity. Thus the core of the jet fluid with a higher velocity has a flatter trajectory and forms the primary jet; the periphery of the jet fluid with a lower velocity forms the plume region," (Arakeri et al., 2000).

The condition of bifurcation is a function of the Reynolds and Grashof numbers as well as the jet transition to turbulence meaning that the jet must remain laminar for bifurcation to occur. The jet is described as a three part jet consisting of the primary jet, the peripheral jet which forms the plume, and the entrained fluid as shown in Figures 11 and 12 of their work. Satyanrayana and Jaluria, 1982, study the jet trajectory of laminar jets and their results conclude that the Reynolds and Grashof numbers are the governing parameters of the jet trajectory. A similar conclusion is drawn from the work of Law et al., 2003. The Reynolds and Grashof number describe the inertial to viscous forces and buoyancy to viscous forces, respectively.

Helmer et al., 2007, study the mixing characteristics of turbulent and laminar vertical buoyant jets via species concentration measurements. Their results indicate that the buoyancy affects the mixing characteristics of the jet and suggests that less fluid is entrained from the ambient relative to non-buoyant jets (Helmer et al., 2007). This is due

to the observed jet/ambient fluid interface of the mean species concentration profiles, noting that is sharper than those observed in non-buoyant jets. They also conclude that the species concentration fluctuations in buoyant jets are weaker than those in non-buoyant jets (Helmer et al., 2007). Their experiments are part of an ongoing research effort that will aid in the development of scalar transport and mixing models in turbulent flow (Helmer et al., 2007).

Summary

The essential components required for FRS measurements are a narrow linewidth laser, absorption filter, and detector. Rayleigh scattering is the molecular scattering of light and occurs due to the protons and electrons within the atom. The scattering occurs at the same frequency as the incident light in the absence of particle motion. The laser supplies the light source and Rayleigh scattering provides the signal to the camera. Continuous and pulsed wave lasers are used in FRS experiments. The signal is filtered with the use of an atomic or molecular absorption filter designed to transmit and block light at different wavelengths. The most common choice for these filters is an iodine filter due to its sharp cut off edges, strong transmission zones and blocking regions, and broad range of transmission zones. The sampling rate of FRS measurements should be optimized to better capture the mixing regions of jets and can be dependent upon the selected camera and/or laser.

Typical jets are exhausted into an ambient fluid and their behavior can be modeled in a simplified way as two dimensional. The jet begins to spread as it is exhausted into the ambient while also entraining the ambient fluid into the jet. Helical

jets are more complicated than the typical jet due to its three dimensional nature and consequently cannot be modeled as a two dimensional jet. The helical motion constructs a jet cross section having five to nine azimuthal fingers. Regardless of the jet type, whether two or three dimensional, the jet spread and mixing regions are generally the primary focus of studying jet behavior.

The behavior of horizontal and vertical buoyant jets is defined in terms of the jet spread, mixing characteristics, and additionally the jet trajectory for horizontal buoyant jets. Buoyant jets are predominantly studied via experimental techniques. The jet trajectory is characterized by non-dimensional numbers in the literature and thus a comparative analysis of experimental results is warranted. Under certain circumstances, a laminar horizontal jet will bifurcate due to the jet buoyancy provided that the jet remains laminar (Arakeri et al., 2000). The mixing characteristics are studied in the referenced literature via species concentration measurements over a broad range of Reynolds numbers and suggests that less fluid is entrained in buoyant jets than in non-buoyant jets (Helmer et al., 2007).

III. Methodology

Chapter Overview

The purpose of this chapter is to describe the procedure for the data acquisition in this research. This ranges from the beginning of the experimental set-up to the end of the data collection. Overhead and cross sectional views of the jet are collected. The experimental setup for the cross sectional view is shown in Figure 7. The role and effects of each experimental component is described herein.

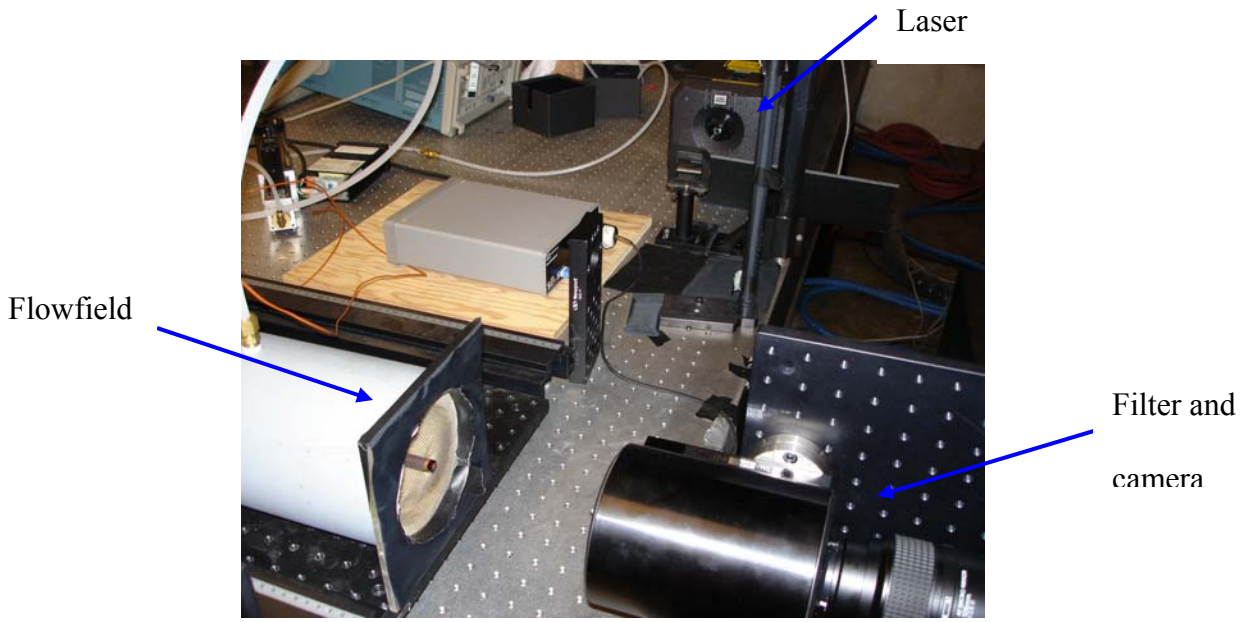

Figure 7. The laser illuminates the flowfield. The filter dissipates unwanted light and the camera collects the signal. Helium exits the copper tube while air co annularly exits the tank at a negligible velocity. In the above setting, the camera is records cross sectional data of the helium jet.

The Experimental Set-Up for FRS

The experimental set-up of the FRS components includes an argon ion laser, an iodine molecular filter, and a PCO.4000 CCD camera.

Laser

The laser for this work is a Coherent Argon Sabre-R Series Ion Laser. The laser rests on a 48 sqft optics table from ThorLabs. The four main components of the laser are the power supply, laser head, heat exchanger, and remote as shown in Figure 8. The power supply distributes the necessary power for each component. The laser head outputs the laser beam. The heat exchanger provides cooling for the laser head and in the passbank in the power supply (Coherent,2001). The laser operates in a wavelength range of 454-515 nm. From Chapter II, the scattering power is proportional to the irradiating intensity of the incoming wave. It is therefore desirable to operate the laser at its maximum power setting in order to strengthen the scattering signal. This laser's maximum power correlates with wavelengths near 514.5 nm and is therefore the selected wavelength for these experiments.

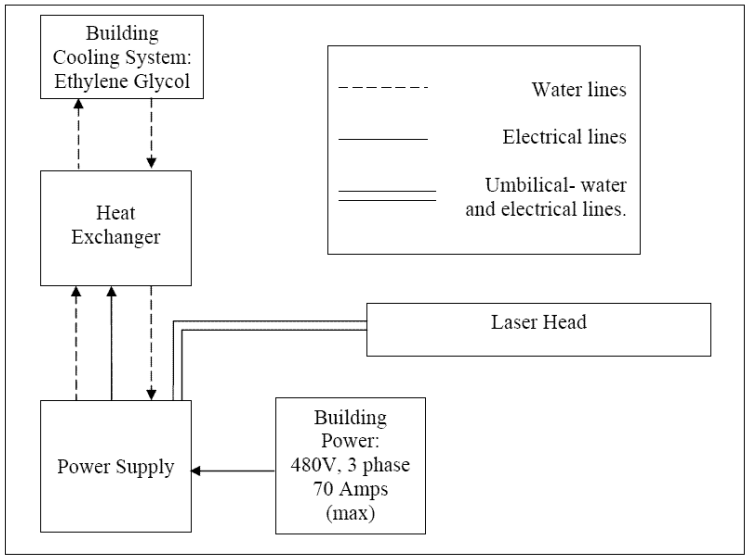

Figure 8. The main components required to operate the laser. The remote, not shown, connects to the power supply and is the user defined interface to the system.

Iodine Filter

As mentioned in Chapter II, an iodine filter is an excellent choice for FRS measurements. The filter is manufactured by Innovative Scientific Solutions Inc (ISSI) and is 3 inches in diameter and 5 inches long. The filter absorption notch is determined experimentally and is discussed later in this chapter.

PCO.4000 CCD and Camera Lens

The PCO.4000 is a 4032x2688 pixel camera with a monochrome or colored CCD imaging sensor. The binning range of the camera is (HxV) 1x1 to 2x8. The manufacturer suggests that a frequency sampling rate of 80 Hz is achievable. The frequency was determined using an oscilloscope and is discussed later in this chapter. A 105 mm, 1:2.8 D AF MICRO NIKKOR camera lens was placed on the camera. The FStop setting is 2.8 and the focused distance is on the order of a foot.

The Experimental Set-Up for the Flowfield

The experimental set-up of the buoyant flowfield includes a stagnation chamber, helium and air supply, and two mass flow controllers.

The stagnation chamber slowly exhausts the co-flow of air while also clamping the co-axial pipe used to create the buoyant jet. The chamber contains a screen at the exhaust used to straighten the air flow. The diameter exit of the chamber is 4 inches.

Air is supplied via the building compressed air system. The system uses Ingersol Rand screw type compressors with an automatic toggle maintaining pressure between 150-200 psig in an externally stored 6000 gallon tank. The air is dried by a series of two

HRM series heatless driers which are preceded by a particulate/coalescing filter. The air pressure entering the feed to the mass flow controller is set at approximately 40 psig. Helium is supplied via approximately a 1 ft diameter x 5 ft length cylindrical tank. The helium pressure entering the feed to the second mass flow controller is set at approximately 60 psig. The helium is directed through a flexible hose which passes through a port on the stagnation chamber located 5 inches upstream of the chamber exit. Fittings are used to redirect the helium through a 90 degree bend and subsequently through a 5 inch long, 0.26 inch inner diameter tube. The tube exit corresponds to the center of the tank exit.

The Alicat Scientific model number MCR-1500SLPM-D is the mass flow controller for setting both the air and helium flow rates. The line pressure feed to the mass flow controller must not exceed 125 psig due to manufacturer specifications.

The experimental procedures entail collecting both unfiltered and filtered images from an overhead view of the jet and collecting only filtered images from the cross sectional view of the jet. The laser is tuned to the appropriate frequency by setting the laser etalon temperature in order to collect the filtered images. The jet is positioned at different axial positions in order to obtain trajectory data of the jet. The camera binning was reduced in order to collect data at lower exposure times.

The pipe exit is axially positioned from the laser beam at 3/8”(x/d = 1.4) to 2.580”(x/d = 9.9) using 315/1000”(x/d = 1.2) increments to observe the top view of the jet. A schematic of this is shown in Figure 9. For the cross sectional view of the jet, the pipe exit is axially positioned 0.50, 1.00, and 2.18 inches (x/d = 1.9, 3.8, 8.4) from the

beam. The velocities of the helium jets and co-flow are 41, 15, and 0.51 ft/s, respectively.

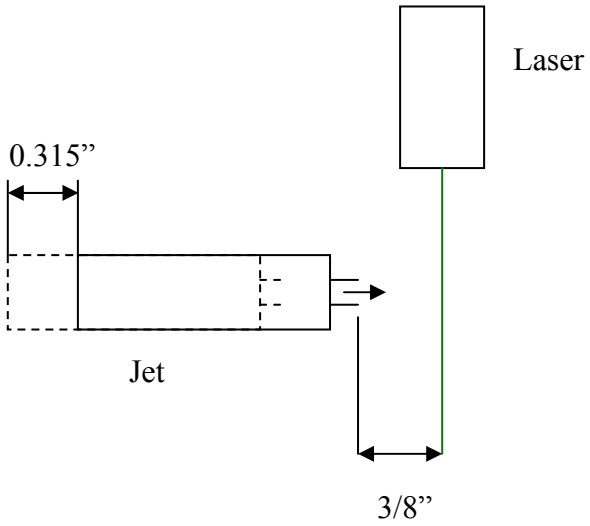

Figure 9. The jet location is varied in 315/1000” increments to collect data at various downstream locations. The data is collected as the jet crosses the laser beam. This is looking down at the set up.

The laser operates at wavelengths in the proximity of 514.5 nm for this study. The manufacture’s power specification for single frequency operation at 514.5 nm is 4.2 W. However during testing, power levels were approximately 8 W. The operating wavelength of the laser is changed by adjusting the etalon temperature. An etalon temperature corresponding to an absorption notch within the filter is found using the technique depicted by Miceli and is shown in Figure 10. A portion of the laser beam is split and is directed towards the filter. The power of the beam through the filter is monitored using a power meter. As the wavelength is varied, the filter begins to transmit and block light at different wavelengths. An absorption notch is found when the power meter readings are relatively low. The etalon temperature used to create the filtered images was 53.9C.

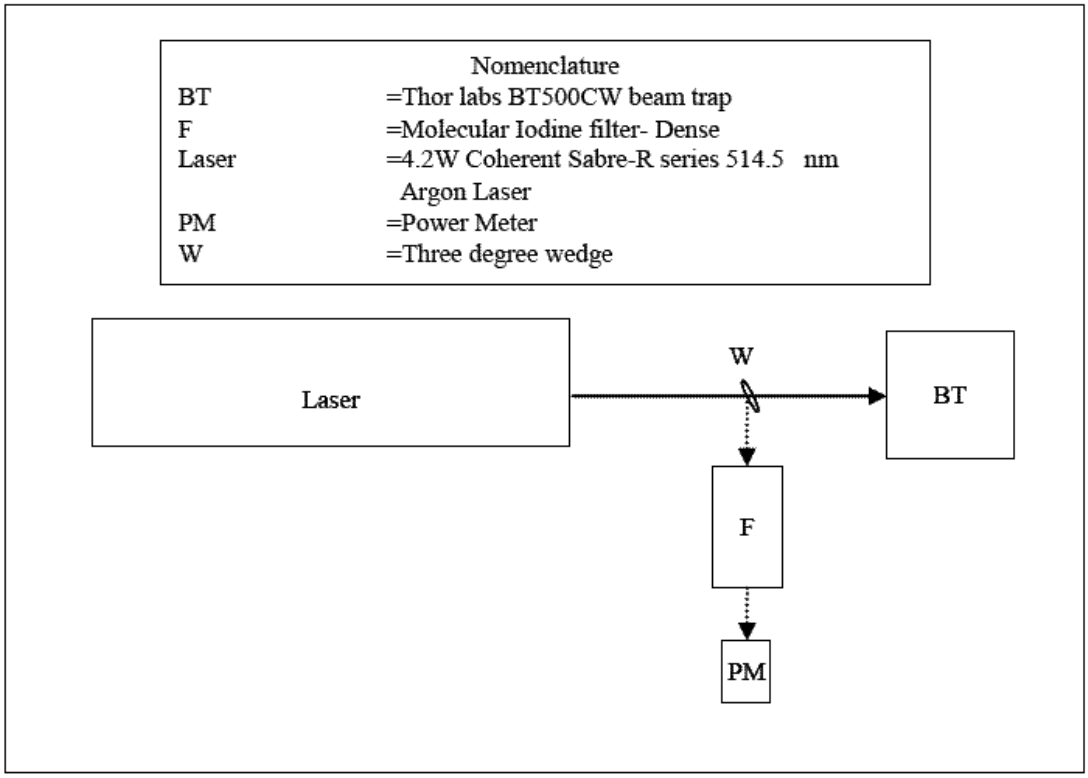

Figure 10. Low readings from the power meter correspond to an absorption notch. The filter will also fluoresce as it blocks light and can be visually observed.

The camera binning and exposure time are optimized to collect data at the fastest sampling rate possible. Data is collected at exposure times ranging from 10-50 ms using a 2x8 binning for the overhead view of the jet. The exposure times are adjusted through the software that controls the camera's operation. The sampling rate, including both the exposure and delay time, is measured by connecting an oscilloscope to the camera's status output exposure port on the camera power supply box while operating the camera. The measured sampling rate is on the order of 20 Hz for the range of exposure times at which data is collected. In the interest of time, a 50 ms exposure time is chosen for data

processing corresponding to a maximum 20 Hz sampling rate for the overhead images. Cross sectional data is collected at a 50 ms exposure time using a 2x2 binning. The corresponding measured sampling rate is 6.5 Hz.

Summary

Filtered and unfiltered images are collected to study the behavior of a buoyant jet. The jet position is varied axially in order to get jet trajectory data. Both overhead and cross sectional views of the jet are collected, albeit more data is collected from the overhead view. The data processing for this research correlates with sampling frequencies of 20 and 6.5 Hz for the overhead and cross sectional views of the jet, respectively. These parameters were chosen for the interest of time and are further mentioned in Chapter IV.

IV. Results and Analysis

Chapter Overview

The purpose of this chapter is to analyze the raw data. Helium concentration measurements at various downstream locations of the jet are presented herein. The concentration measurements reveal that the helium jet mixing behavior with the ambient fluid exhibits expulsion of core fluid at several circumferential locations under certain operating conditions and is addressed in a subsequent section of this chapter. The core jet trajectory is a function of the Reynolds and Grashof numbers and coincides with the data in the referenced literature. Various camera exposure times and camera binnings are investigated to increase the data acquisition sampling rate. The effectiveness of the filter is examined by comparing both unfiltered and filtered images.

Results from Images

The raw data are image files capturing the Rayleigh scattering signal of the helium jet and co-flow of air expulsing into the ambient. The image files yield intensity values at corresponding pixel locations. The collected intensity values are a function of the Rayleigh scattering signal and thus discriminate between the gaseous components. Due to the small Rayleigh scattering cross section of helium as compared to air, the lower intensity values will correlate with high helium concentration measurements while the larger intensity values will correlate with higher air concentration measurements.

The image binning for this research varies from 2x2 to 2x8. The exposure times vary from 10 ms to 50 ms. Figure 11 and Figure 12 display unfiltered and filtered sample

images collected from an overhead view of the jet with the helium mass flow rate set to 25 SLPM, corresponding to a Reynolds number of 667 with a velocity of 41 ft/s. The helium jet and co-flow of air traverse through the laser beam as shown. Figure 13 is a sample image collected from a frontal view of the jet, corresponding again to a Reynolds number of 667 with a velocity of 41 ft/s.

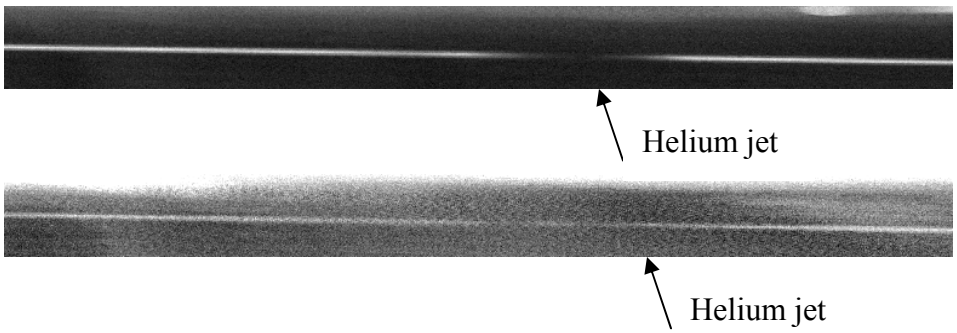

Figure 11. Unfiltered Data collected 1.005" downstream (x/d = 3.9) of the jet at 50 ms exposure time and 0.750" downstream (x/d = 2.9) of the jet at 10 ms exposure time, respectively. The helium jet corresponds with the lower intensity values along the beam. The image binning is 2x8.

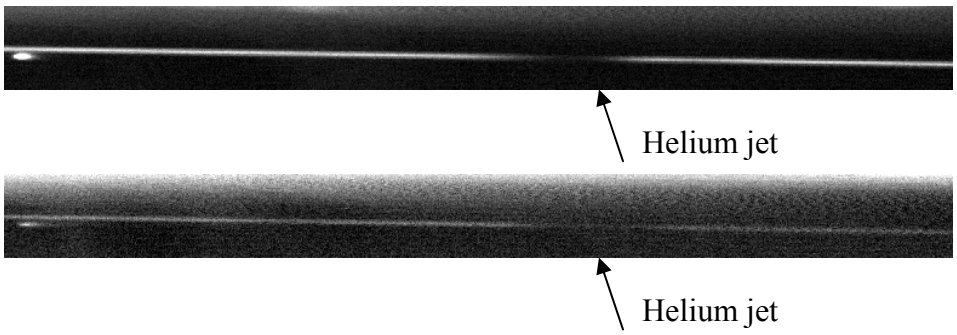

Figure 12. Filtered Data collected 1.005" downstream (x/d = 3.9) of the jet at 50 and 10 ms exposure times, respectively. The filter reduces the noise/signal ratio and the 10 ms exposure time data shows an improvement with the use of a filter.

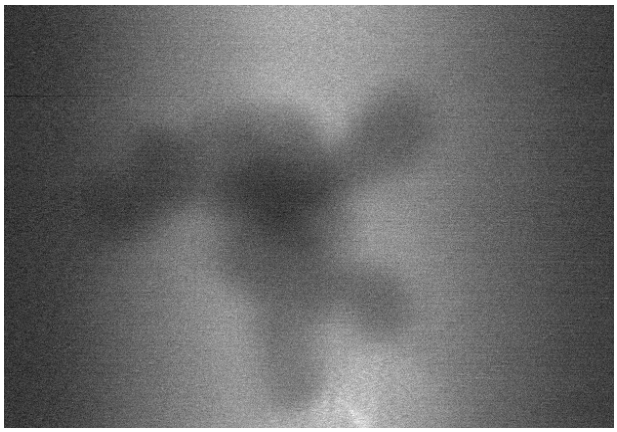

Figure 13. Filtered data of the jet cross section at 0.5" (x/d = 1.9) downstream and a 50 ms exposure time. The image binning is 2x2 and the flowfield is illuminated using a laser sheet.

Helium Concentration Measurements from the Overhead View

The scattered power collected in FRS measurements from a gaseous mixture is commonly written as,

$$I \propto E_0 \sum_i X_i \sigma_i \tag{2}$$

where I is the collected power, E_0 is the irradiating intensity, X is the species mole fraction, and σ is the Rayleigh scattering cross section. For the experiment at hand, noting that the air and helium mole fractions add to one, a subtraction of the background intensities from each signal in combination with Equation (2) yields the helium concentration fraction

$$X_{HE} = \frac{1-(I_{HE}-BG_{HE})/(I_{AIR}-BG_{AIR})}{1-\sigma_{HE}/\sigma_{AIR}} \tag{3}$$

where I is the collected power, BG is the background power, and σ is the Rayleigh scattering cross section. Data was collected without the helium jet on to measure the scattered energy from air (I_{AIR}) only. The helium to air Rayleigh scattering cross section

ratio is 1.4 percent (Lee, Won, Jin, and Chung). The background intensity values correspond to the average intensity values over the sample data range along a straight path parallel to the laser beam near the bottom of each image.

The helium concentration fractions presented in this chapter are averaged over 100 images collected at 20 Hz. For the purposes of the figures within this section this is described as a time-averaged image. The 20 Hz sampling rate correlates with a 50 ms exposure time and a 2x8 binning. These parameters were chosen based on the image clarity as shown in Figure 11 and Figure 12 and the relative simplicity of processing the data. The corresponding standard deviation of concentration measurements over the 100 images is presented. Note that this value for standard deviation does not properly account for fluctuations which take place within the exposure time (50 ms). For this reason, the spatial regions with high values of standard deviation correspond to locations where fluctuations with relatively large time scales exist. The exceedingly large spikes in the standard deviation plots are indicative of particles in the flowfield and are thus clipped in the plots to focus on the mixing region of the jet.

Figure 14 displays the unfiltered and filtered data collected at 1.005 inches downstream of the tube exit (x/d = 3.9). The peak mean helium concentration is 0.94 and 0.92 with a standard deviation of 0.038 and 0.035 for the unfiltered and filtered data, respectively.

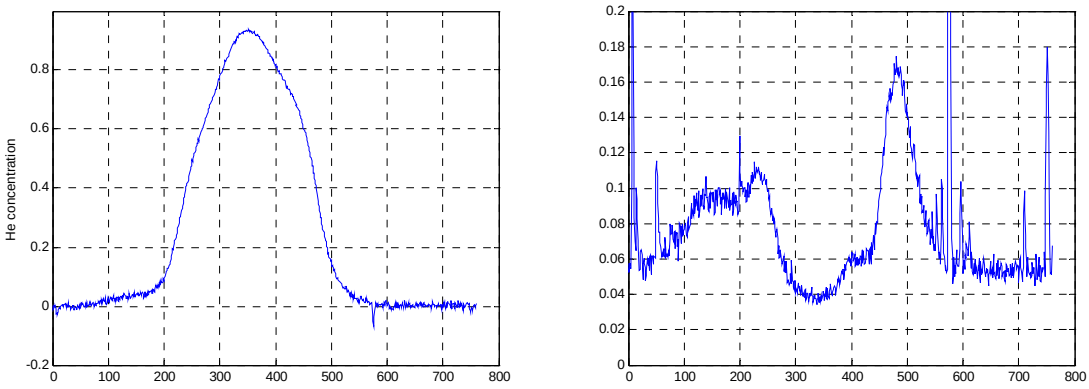

Figure 14. Time averaged helium concentration fraction and corresponding standard deviation. The graph is generated from unfiltered data. The downstream location is 1.005" (x/d = 3.9). The flow rate is 25 SLPM. The x axis is given in pixels where the tube diameter is equated to 180 pixels.

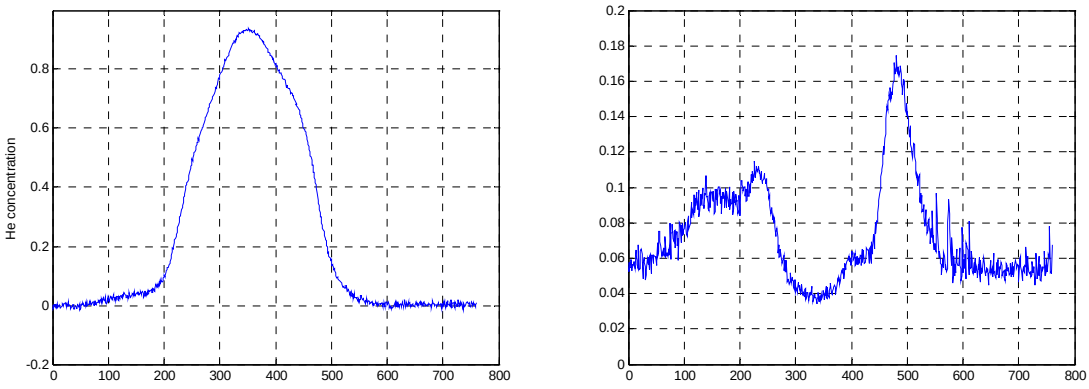

Figure 15. Time averaged helium concentration fraction and corresponding standard deviation. The graph is from unfiltered data. The downstream location is 1.005" (x/d = 3.9). The flow rate is 25 SLPM. From Figure 14, data outside of 6 standard deviations has been set to the mean value for simplicity and is presented here. Note the comparison between Figure 14 and Figure 15. They are the same graphs but with Figure 15 taking into account the statistical anomalies. The x axis is given in pixels where the tube diameter is equated to 180 pixels.

Although care was taken to ensure a particle free flowfield with the use of co-annularly flowed air , it is evident from the standard deviation plot of Figure 14 that some particles entered the flowfield at various times during the data collection. This becomes even more evident at the relatively further downstream locations. Data was collected at different x/d locations varying from 1.4 to 9.9. Figure 15 is an attempt to clean up the raw data measurements by accounting for the particles within the flowfield. Data outside of six standard deviations is considered a statistical anomaly, an outlier in the data, and has been set to the mean value for simplicity. The clean result for the x/d location corresponding to 3.9 is shown in Figure 15 and can be compared to Figure 14. It is evident from processing the data in this manner that an improvement in the data representation is displayed. This process was applied to every x/d location and the results are shown in Figure 16 - Figure 23.

Figure 16 displays the unfiltered and filtered data while accounting for the outliers at 0.375 inches downstream of the tube exit (x/d = 1.4). The peak mean helium concentration is 0.99 and 0.90 with a standard deviation of 0.023 and 0.044 for the unfiltered and filtered data, respectively. The filtered data is biased due to the severity of the reflections which results in the low helium concentration fractions.

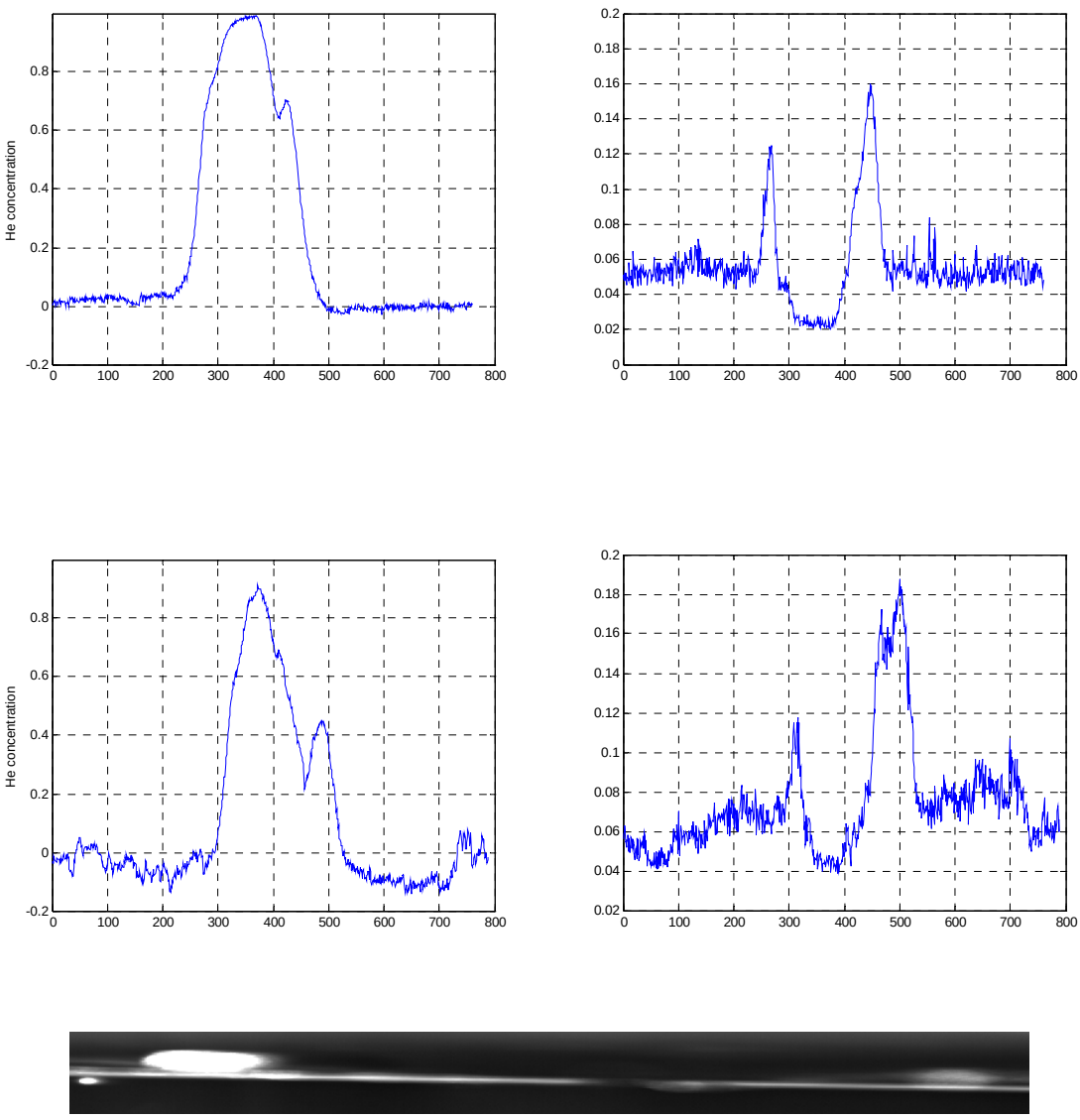

Figure 16. Time averaged helium concentration fractions and corresponding standard deviation. The top graphs are unfiltered and the bottom graphs are filtered. The filtered graphs are biased due to the severity of the reflections as shown in the above image file. The downstream location is 0.375" (x/d = 1.4). 46/76000 and 7/78800 outliers are set to the mean value, respectively. The flow rate is 25 SLPM. The x axis is given in pixels where the tube diameter is equated to 180 pixels.

Figure 17 displays the unfiltered and filtered data while accounting for the outliers at 0.690 inches downstream of the tube exit (x/d = 2.7). The peak mean helium concentration is 0.96 and 0.98 with a standard deviation of 0.035 and 0.038 for the unfiltered and filtered data, respectively.

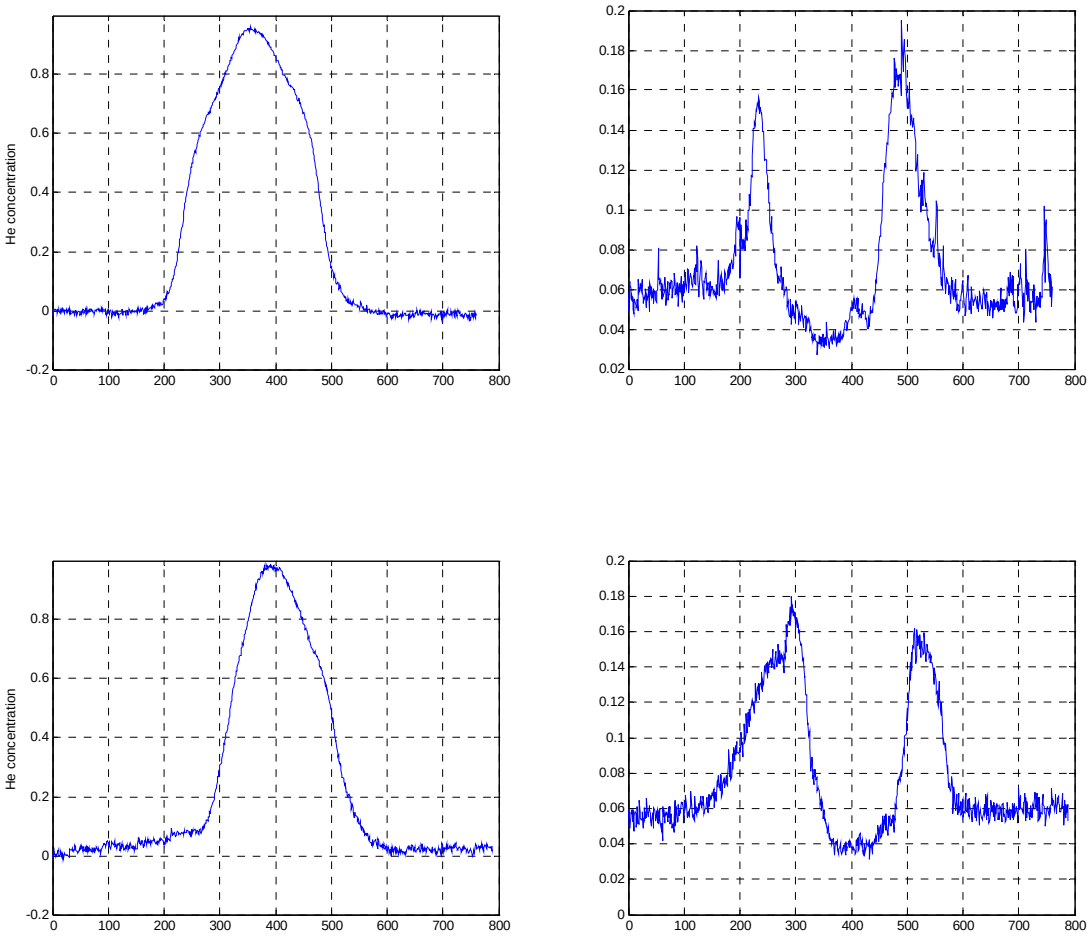

Figure 17. Time averaged helium concentration measurements and corresponding standard deviation. The top graphs are unfiltered and the bottom graphs are filtered. The downstream location is 0.690" (2.7). 46/76000 and 0/78800 outliers are set to the mean value, respectively. The flow rate is 25 SLPM. The x axis is given in pixels where the tube diameter is equated to 180 pixels.

Figure 18 displays the unfiltered and filtered data while accounting for the outliers at 1.005 inches downstream of the tube exit (x/d = 3.9). The peak mean helium concentration is 0.94 and 0.92 with a standard deviation of 0.038 and 0.035 for the unfiltered and filtered data, respectively.

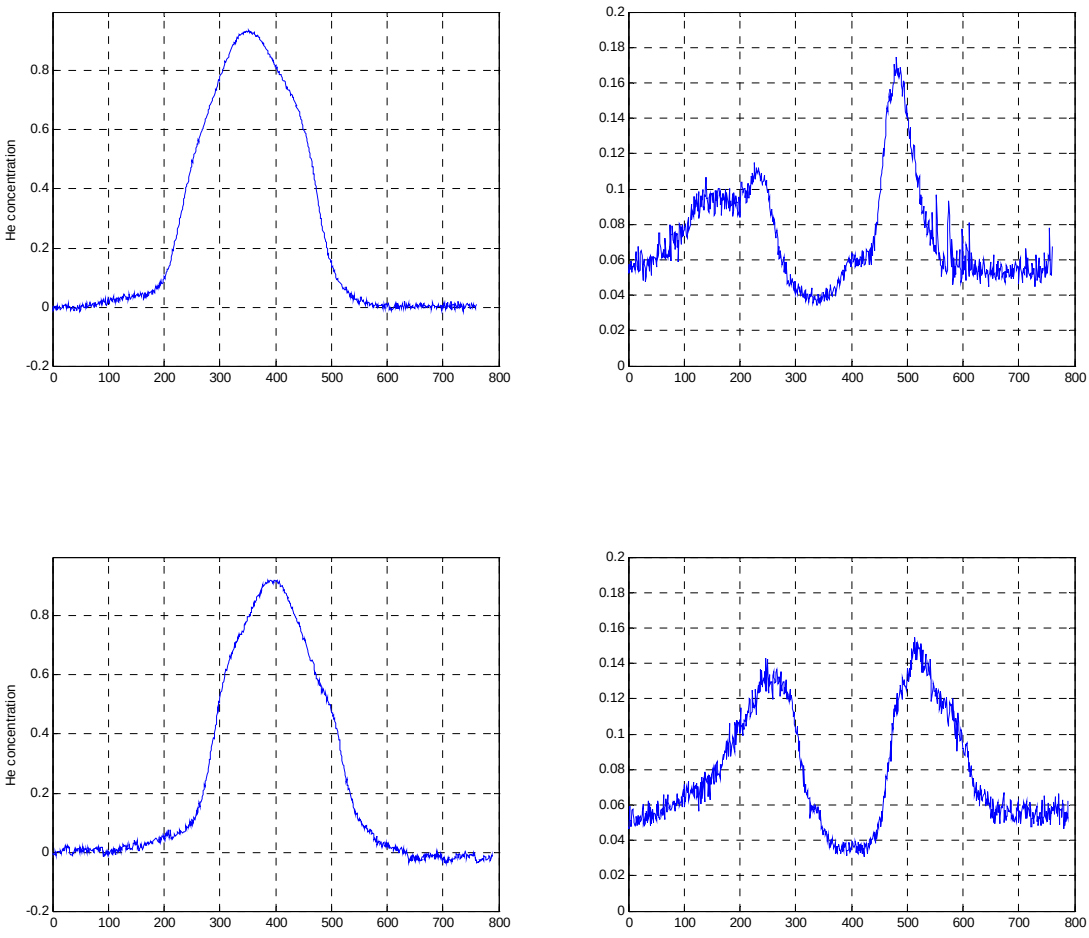

Figure 18. Time averaged helium concentration measurements and corresponding standard deviation. The top graphs are unfiltered and the bottom graphs are filtered. The downstream location is 1.005" (x/d = 3.9). 51/76000 and 0/78800 outliers are set to the mean value, respectively. The flow rate is 25 SLPM. The x axis is given in pixels where the tube diameter is equated to 180 pixels.

Figure 19 displays the unfiltered and filtered data while accounting for the outliers at 1.320 inches downstream of the tube exit (x/d = 5.1). The peak mean helium concentration is 0.87 and 0.82 with a standard deviation of 0.040 and 0.038 for the unfiltered and filtered data, respectively.

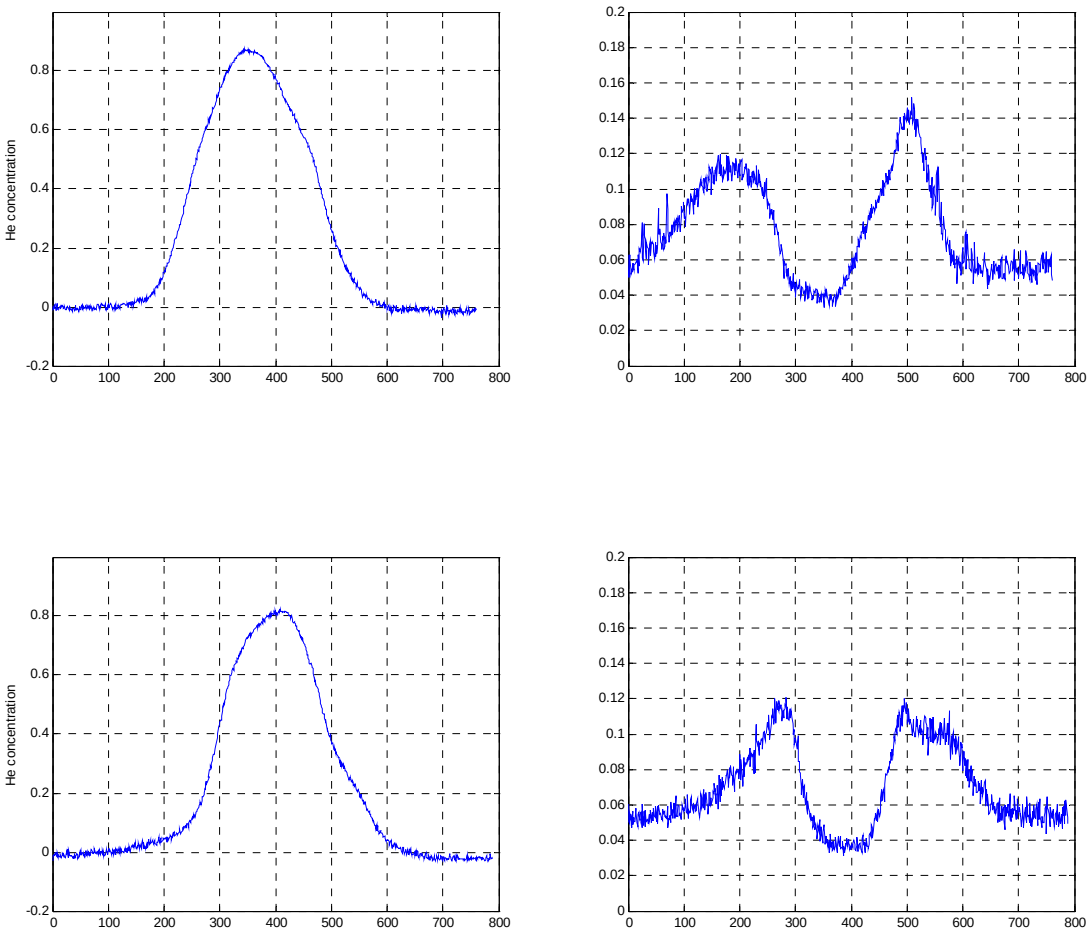

Figure 19. Time averaged helium concentration measurements and corresponding standard deviation. The top graphs are unfiltered and the bottom graphs are filtered. The downstream location is 1.320" (x/d = 5.1). 42/76000 and 0/78800 outliers are set to the mean value, respectively. The flow rate is 25 SLPM. The x axis is given in pixels where the tube diameter is equated to 180 pixels.

Figure 20 displays the unfiltered and filtered data while accounting for the outliers at 1.635 inches downstream of the tube exit (x/d = 6.3). The peak mean helium concentration is 0.82 and 0.79 with a standard deviation of 0.036 and 0.040 for the unfiltered and filtered data, respectively.

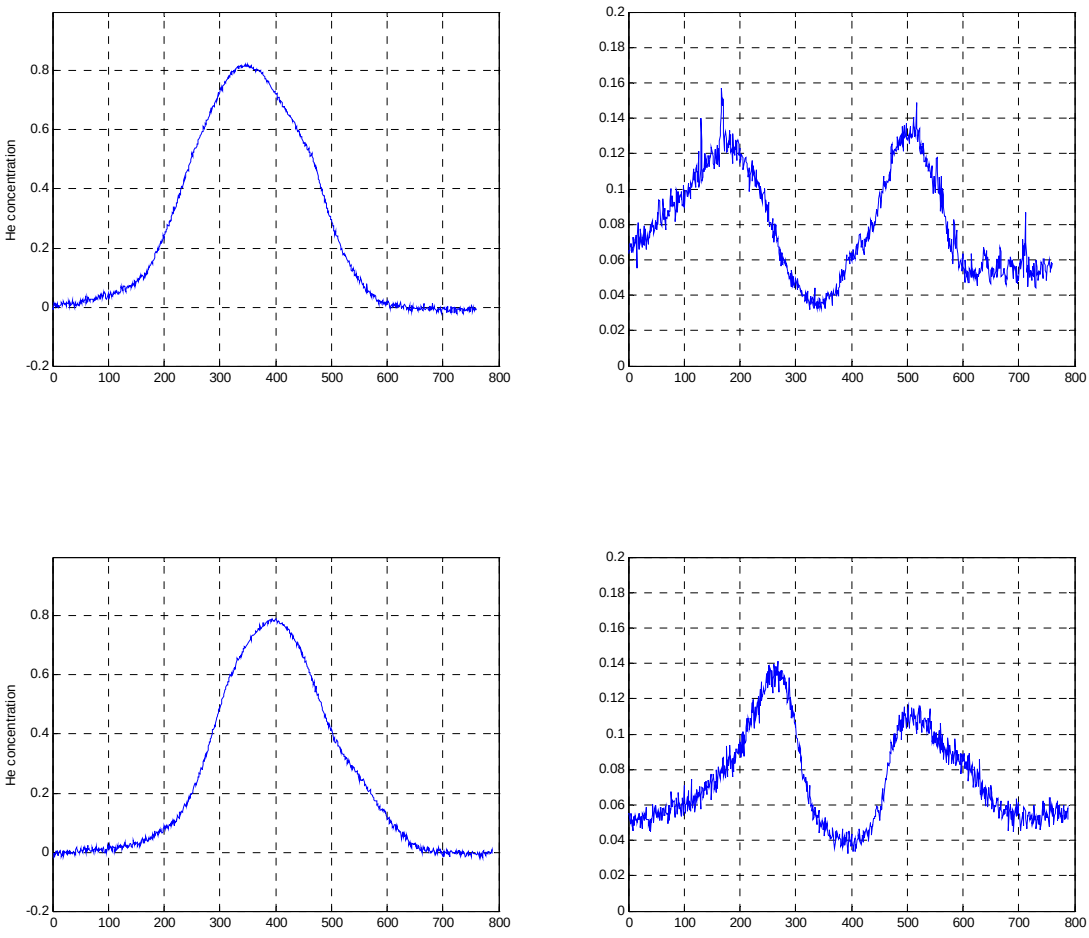

Figure 20. Time averaged helium concentration measurements and corresponding standard deviation. The top graphs are unfiltered and the bottom graphs are filtered. The downstream location is 1.635" (x/d = 6.3) 28/76000 and 0/78800 outliers are set to the mean value, respectively. The flow rate is 25 SLPM. The x axis is given in pixels where the tube diameter is equated to 180 pixels.

Figure 21 displays the unfiltered and filtered data while accounting for the outliers at 1.950 inches downstream of the tube exit (x/d = 7.5). The peak mean helium concentration is 0.77 and 0.74 with a standard deviation of 0.040 and 0.040 for the unfiltered and filtered data, respectively.

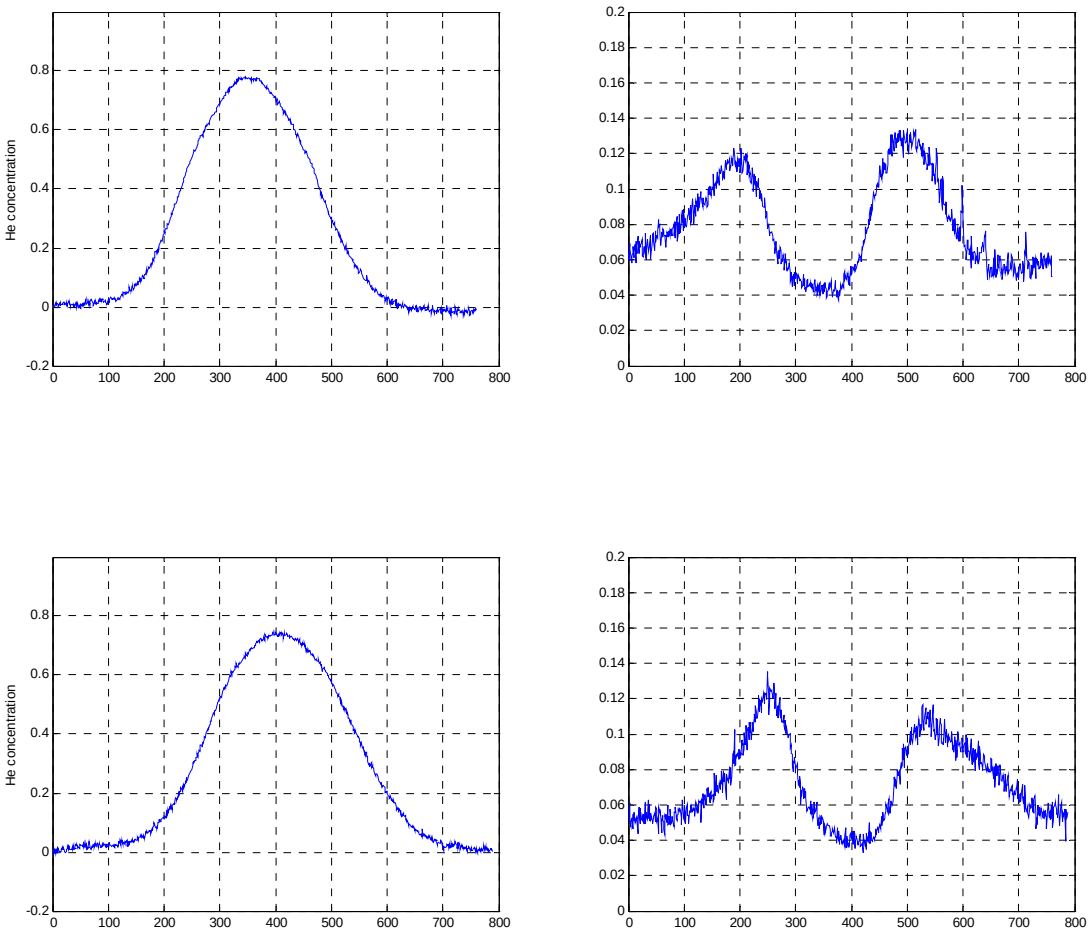

Figure 21. Time averaged helium concentration measurements and corresponding standard deviation. The top graphs are unfiltered and the bottom graphs are filtered. The downstream location is 1.950" (x/d = 7.5). 25/76000 and 0/78800 outliers are set to the mean value, respectively. The flow rate is 25 SLPM. The x axis is given in pixels where the tube diameter is equated to 180 pixels.

Figure 22 displays the unfiltered and filtered data while accounting for the outliers at 2.265 inches downstream of the tube exit (x/d = 8.7). The peak mean helium concentration is 0.75 and 0.70 with a standard deviation of 0.038 and 0.040 for the unfiltered and filtered data, respectively. There are too many particles within the flowfield for the filtered data and hence the signal is dominated by Mie scattering which explains the poor results on the right portion of the graph.

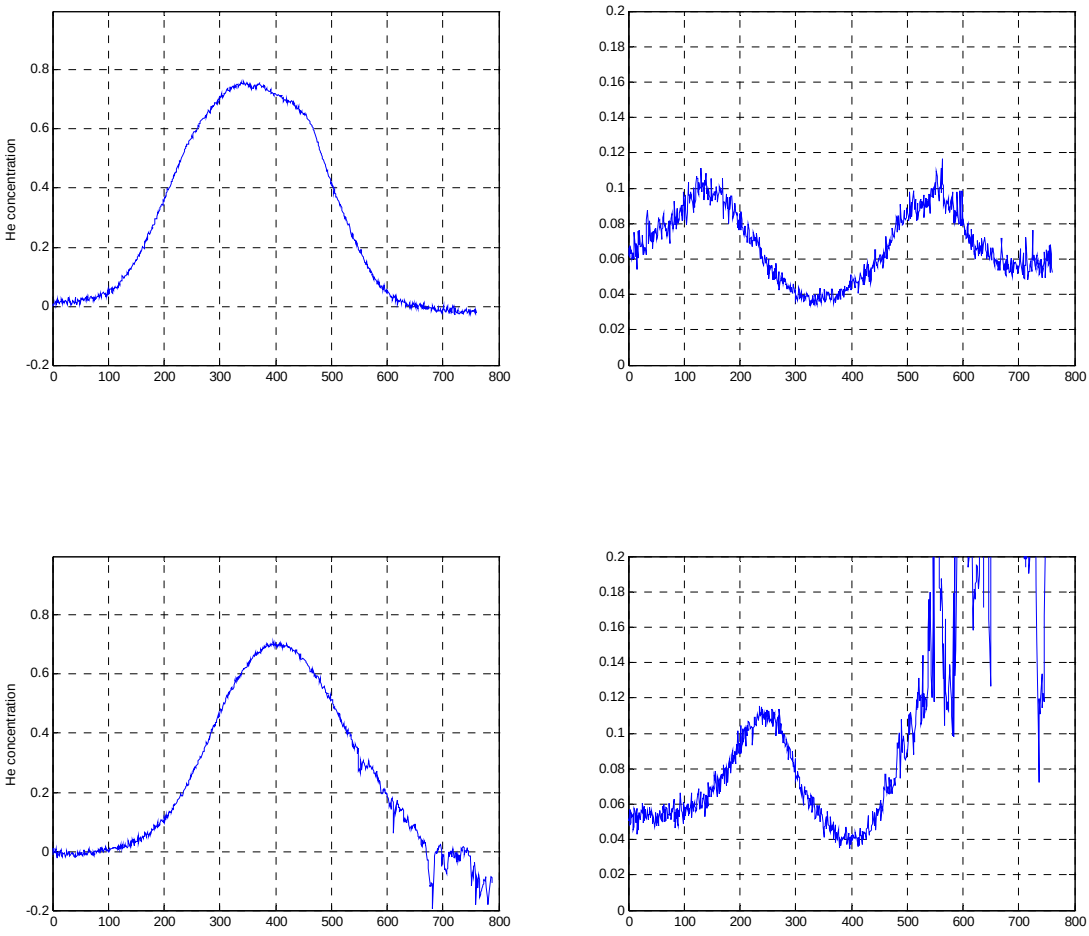

Figure 22. Time averaged helium concentration measurements and corresponding standard deviation. The top graphs are unfiltered and the bottom graphs are filtered. The downstream location is 2.265" (x/d = 8.7). 62/76000 and 289/78800 outliers are set to the mean value, respectively. The flow rate is 25 SLPM. The x axis is given in pixels where the tube diameter is equated to 180 pixels.

Figure 23 displays the unfiltered and filtered data while accounting for the outliers at 2.580 inches downstream of the tube exit (x/d = 9.9). The peak mean helium concentration is 0.73 and 0.68 with a standard deviation of 0.040 and 0.050 for the unfiltered and filtered data, respectively.

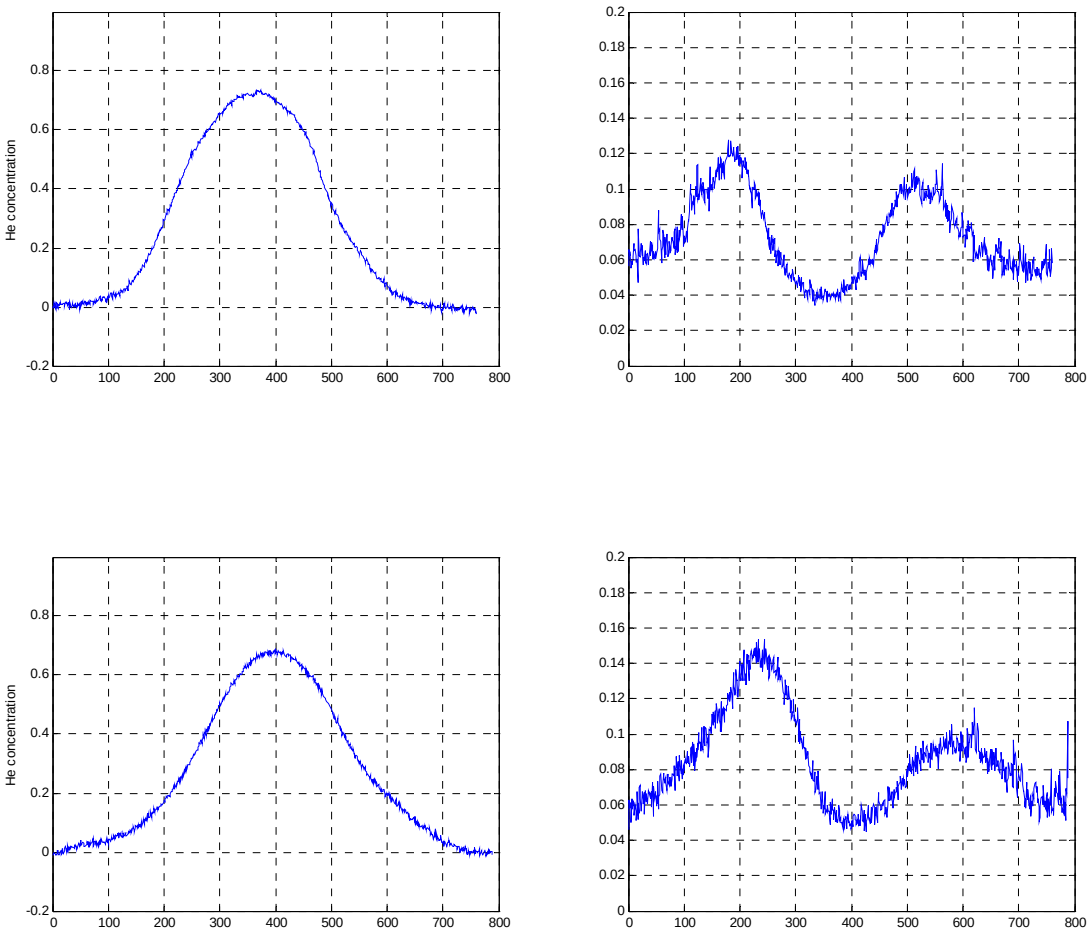

Figure 23. Time averaged Helium concentration measurements and corresponding standard deviation. The top graphs are unfiltered and the bottom graphs are filtered. The downstream location is 2.580" (x/d = 9.9). 38/76000 and 30/78800 outliers are set to the mean value, respectively. The flow rate is 25 SLPM. The x axis is given in pixels where the tube diameter is equated to 180 pixels.

The general trend of concentration measurements reveal that the entrainment with the ambient fluid increases further downstream of the jet, as expected. The standard deviation plots reveal the core and mixing regions of the jet and are in the range of 0 to 20 percent, consistent with the literature (Borg et al., 2001). The data from the filtered images has less noise to signal ratio and is cleaner than the data from the unfiltered images. The peak concentration measurements vary slightly between the unfiltered and filtered images but are within reason based on the core standard deviation values and is shown in Table 1. The slight variation of the location at which the peak concentration occurs between the unfiltered and filtered images may be due to a camera movement between the two data sets.

Table 1. Peak mean helium concentration measurements and standard deviations at data collected at a 50 ms exposure time.

Downstream Position (in, x/d)	Peak X_{He} Unfiltered	Stand Dev Unfiltered (core)	Peak X_{He} Filtered	Stand Dev Filtered (core)
0.375, 1.4	0.99	0.023	0.90	0.044
0.690, 2.7	0.96	0.035	0.98	0.038
1.005, 3.9	0.94	0.038	0.92	0.035
1.320, 5.1	0.87	0.040	0.82	0.038
1.635, 6.3	0.82	0.036	0.79	0.040
1.950, 7.5	0.77	0.040	0.74	0.040
2.265, 8.7	0.75	0.038	0.70	0.040
2.580, 9.9	0.73	0.040	0.68	0.050

Table 2 presents the number of outliers within each downstream location of the jet for both the unfiltered and filtered images and is a measure of the associated noise to signal ratio and is also accounting for the particles in the flowfied. With the particles appropriately accounted for, it is even more evident from the standard deviation plots that the filter has reduced the noise to signal ratio of the data and presents cleaner plots than the unfiltered images.

Table 2. The outliers in the data outside of 6 standard deviations. The number of outliers for the filtered data at x/d = 8.7 is indicative of too many particles in the flowfied.

Downstream Location (in, x/d)	Unfiltered Outliers	Filtered Outliers
0.375, 1.4	46/76000	7/78800
0.690, 2.7	46	0
1.005, 3.9	51	0
1.320, 5.1	42	0
1.635, 6.3	28	0
1.950, 7.5	25	0
2.265, 8.7	62	289
2.580, 9.9	38	30

Helium Concentration Measurements from the Frontal View

The previous measurements are from an overhead view of a laser beam intersecting the jet. The measurements displayed in this section are from a cross sectional view of the jet. The concentration measurements are calculated for each point in the 2D plane using Equation (3) and are time averaged over 100 images. The

background values are the average intensity values below the laser sheet as shown in Figure 24. Although the intensity varies across the laser sheet and thus the background values should also vary, constant background values produce helium concentration measurements consistent with the measurements from the overhead view of the jet at corresponding downstream positions. The exposure time is 50 ms, corresponding to a sampling rate of 6.5 Hz, and the camera binning is 2x2.

Standard deviation plots are also presented and display higher core standard deviation values than the overhead data. This is due to the greater noise to signal ratio for the data collected using a laser sheet versus the data collected using a laser beam. This is expected due to the large variation of signal intensities as a result of creating a laser sheet. The higher noise to signal ratio also explains why the standard deviation plots reveal meaningless data outside of the jet area in which there is no signal at all.

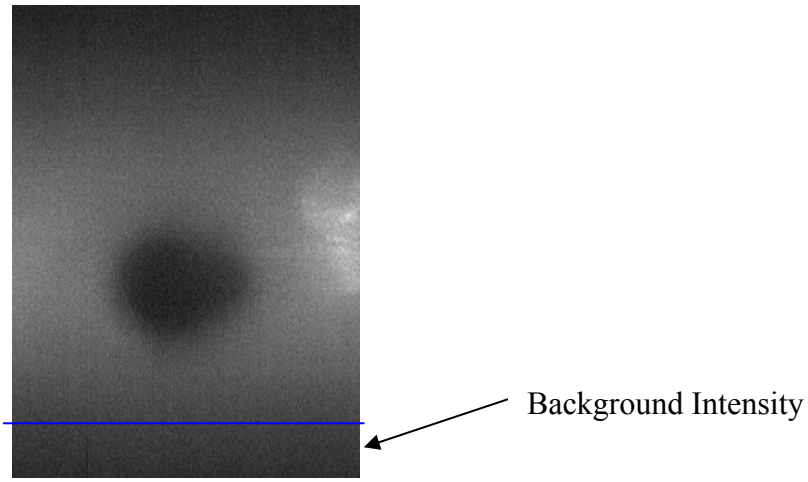

Figure 24. A sample image pinpointing the background intensity values. The background image was generated by replicating the bottom portion of the collected image and creating an artificial image the same size as the collected image.

Figure 25 displays mean helium concentration fractions and standard deviation data from two different jet velocities, 41 and 15 ft/s, respectively at a downstream distance of 0.5 inches (x/d = 1.9). These velocities correspond to a Reynolds number of 667 and 238, respectively. The core concentration measurements are close to one and are consistent with the measurements calculated from the unfiltered and filtered top view data of the jet at 41 ft/s, ranging from 0.98 to 0.99 at 0.690 and 0.375 inches downstream of the tube exit (x/d = 2.7, 1.4), respectively. The unfiltered data was used in lieu of the filtered data at 0.375 inches downstream due to the associated bias as discussed in Figure 16. Data was not collected at 15 ft/s from a top view of the jet.

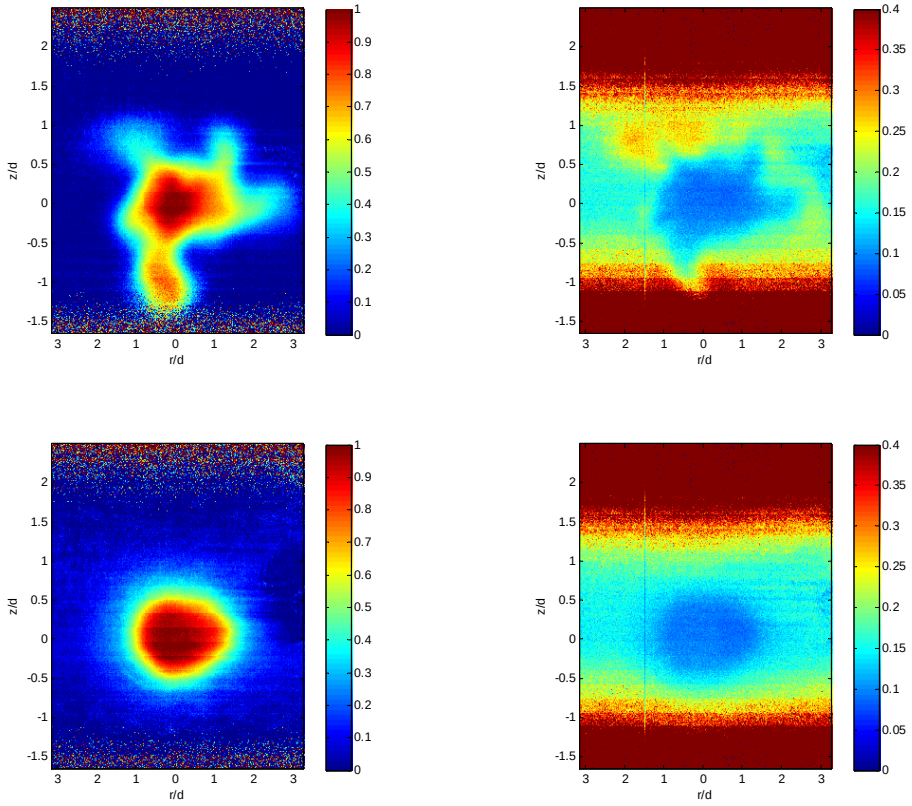

Figure 25. Time averaged helium concentration measurements and standard deviation. The downstream location is 0.5" (x/d = 1.9) and the jet velocity is 41 and 15 ft/s, respectively.

Figure 26 displays mean helium concentration measurements and standard deviation data at a jet velocity of 41 ft/s and downstream distance of an inch (x/d = 3.8). This velocity corresponds to a Reynolds number of 667. The core concentration measurements are approximately 0.90 and are consistent with the measurements calculated from the filtered top view data of the jet at 41 ft/s, a value corresponding to 0.92 at 1.005 inches downstream of the tube exit (3.9). The jet standard deviation values range from approximately 10 % in the core region to 20% in the outer region.

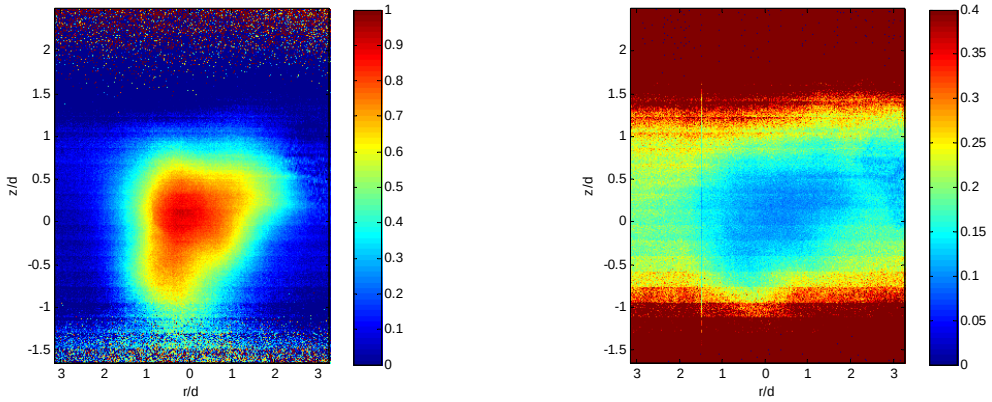

Figure 26. Time averaged helium concentration measurements and standard deviation. The downstream location is 1.0" (x/d = 3.8) and the jet velocity is 41 ft/s.

Figure 27 displays mean helium concentration measurements and standard deviation data from two different jet velocities, 41 and 15 ft/s, respectively at a downstream distance of 2.18 inches (x/d = 8.1). These velocities correspond to a Reynolds number of 667 and 238, respectively. The core concentration measurements are approximately 0.75 and are comparable with the measurements calculated from the filtered top view data of the jet at 41 ft/s, ranging from 0.75 to 0.70 at 1.950 and 2.265 inches downstream of the tube exit (x/d = 7.5, 8.7), respectively. Data was not collected at 15 ft/s from an overhead view of the jet. The standard deviation data values range from approximately 10% in the core region to 20% in the outer region.

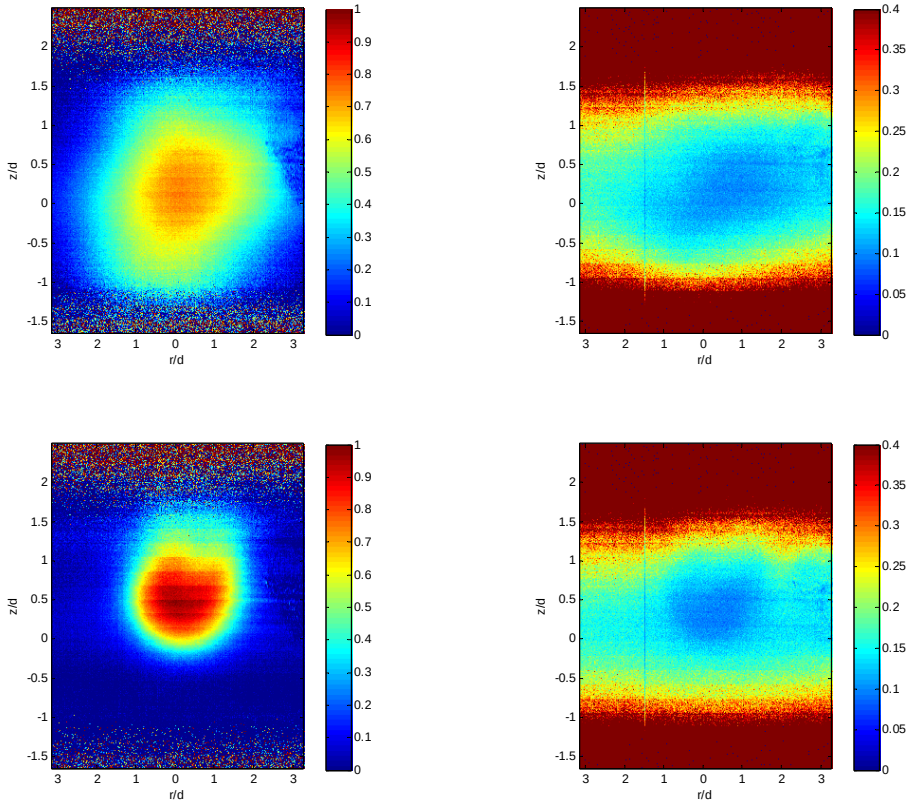

Figure 27. Time averaged helium concentration measurements and standard deviation. The downstream location is 2.18" (x/d = 8.4) and the jet velocity is 41 and 15 ft/s, respectively.

The difference in mixing patterns between the jets of different Reynolds numbers in Figure 25 is dramatic and requires a discussion before going on to the next subject. Sequential data at 6.5 Hz with an exposure time of 50 ms is shown in Figure 28-Figure 31 to illustrate the jet behavior. The relatively high speed jet (Reynolds number of 667) is compared to the low speed jet (Reynolds number of 238). The five azimuthal fingers are indicative of a helical mode jet (Chao et al., 2000).

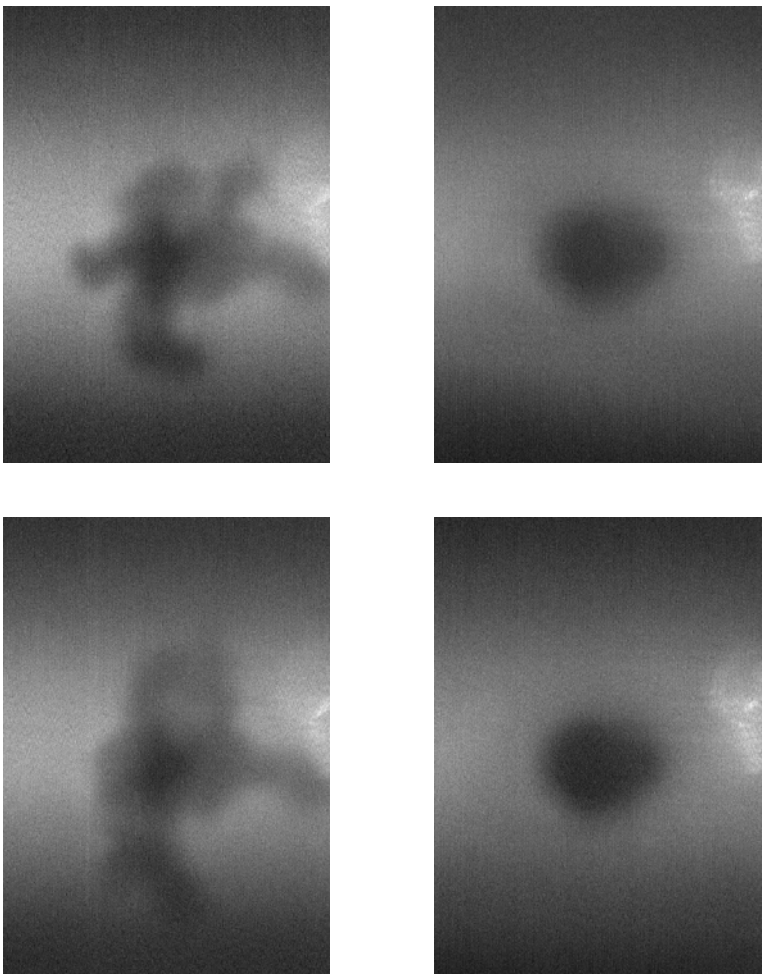

Figure 28. Sequenced data at a sampling rate of 6.5 Hz. The Reynolds numbers on the left and right are 667 and 238, respectively. The downstream location is 0.5" (x/d = 1.9). The images shown is 1 and 2 of the sequence, respectively.

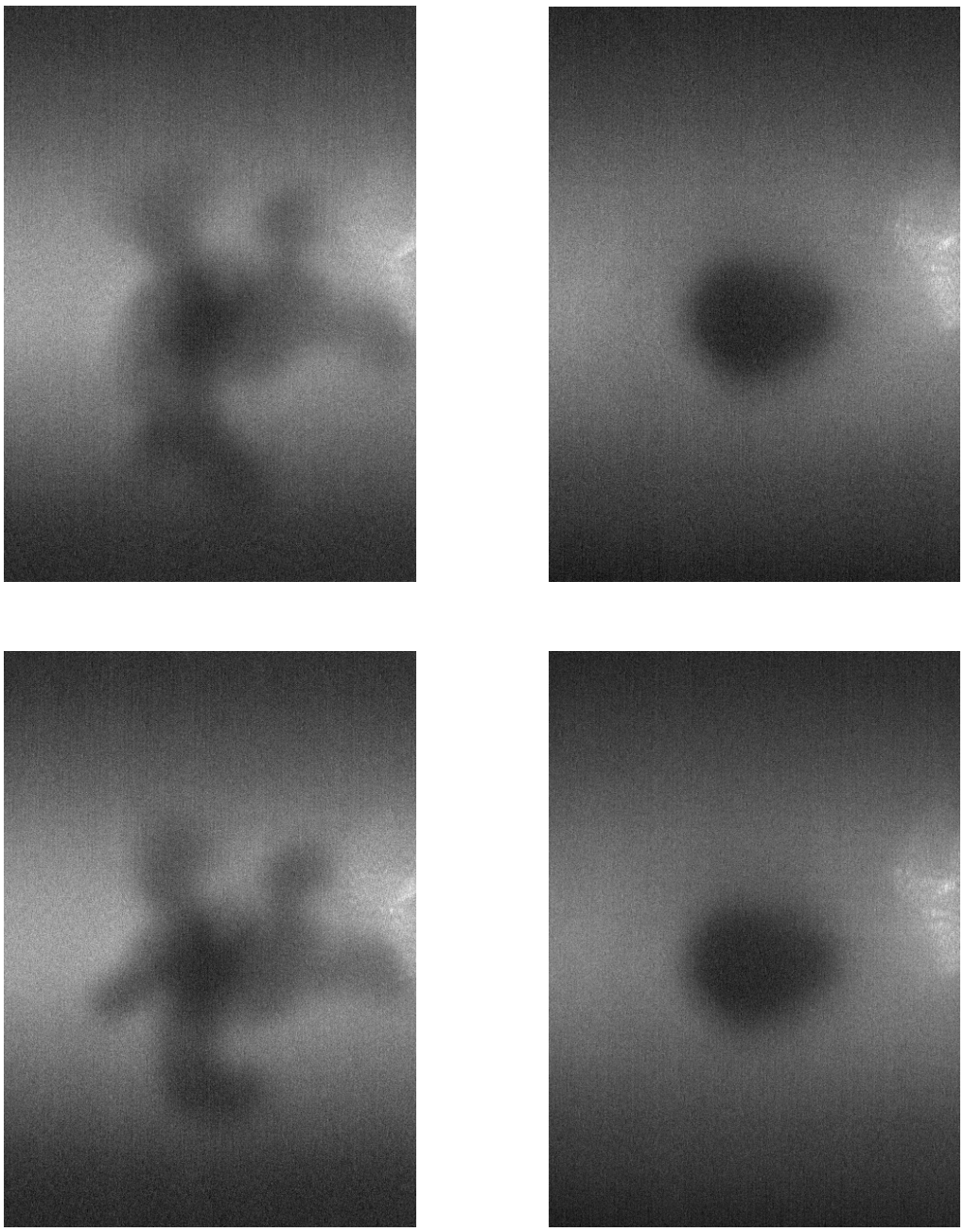

Figure 29. Sequenced data at a sampling rate of 6.5 Hz. The Reynolds numbers on the left and right are 667 and 238, respectively. The downstream location is 0.5" (x/d = 1.9). The images shown is 3 and 4 of the sequence, respectively.

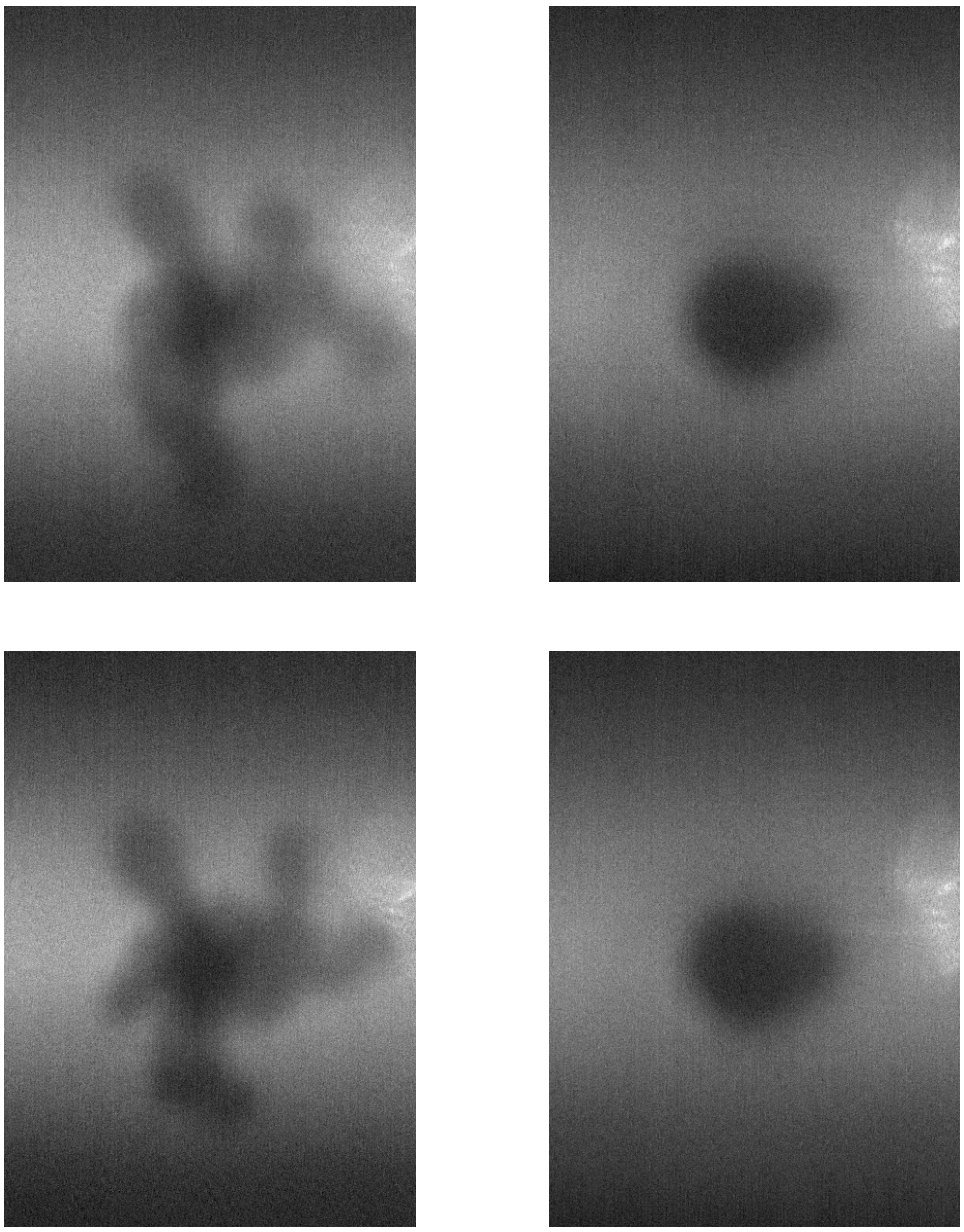

Figure 30. Sequenced data at a sampling rate of 6.5 Hz. The Reynolds numbers on the left and right are 667 and 238, respectively. The downstream location is 0.5" (x/d = 1.9). The images shown is 5 and 6 of the sequence, respectively.

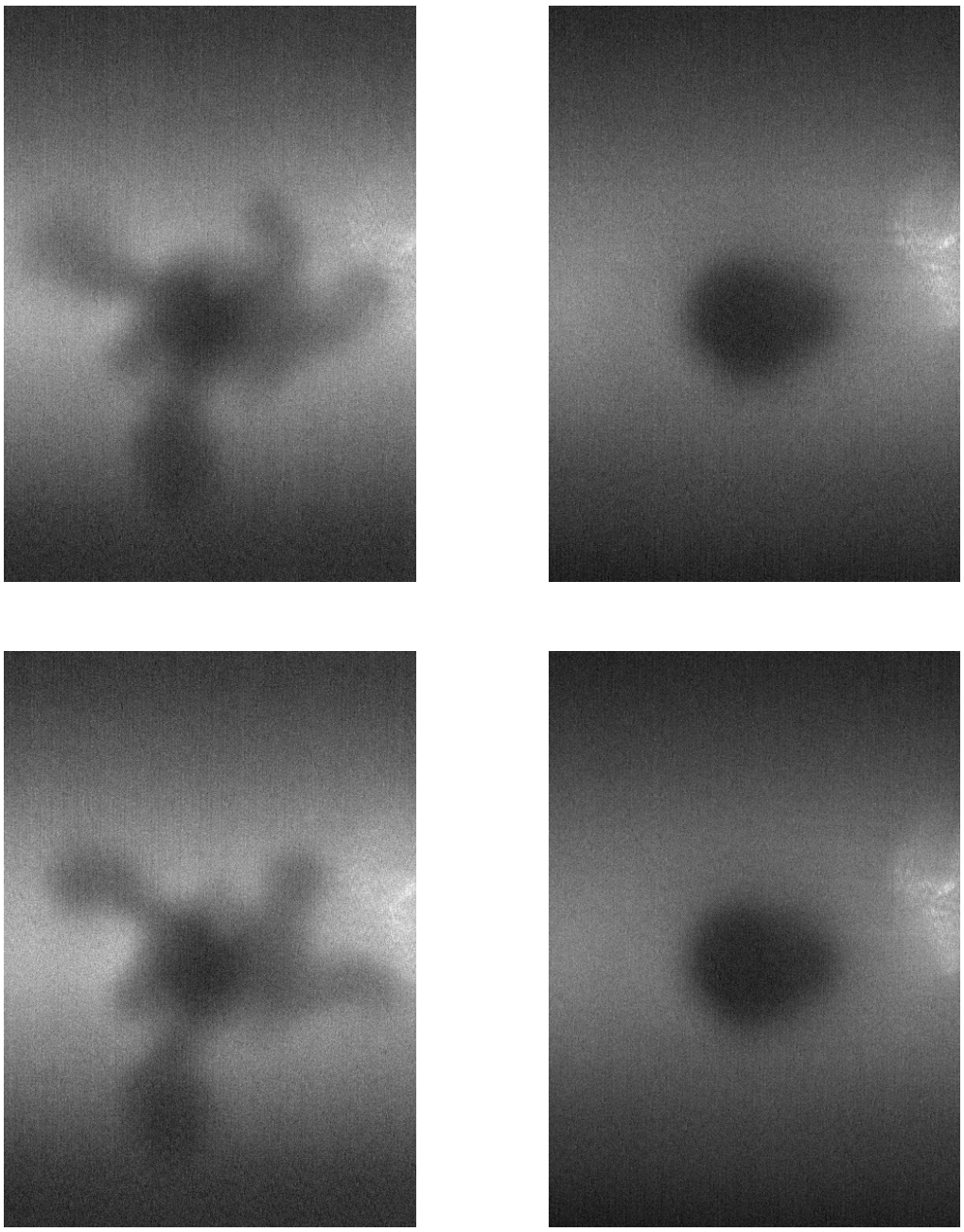

Figure 31. Sequenced data at a sampling rate of 6.5 Hz. The Reynolds numbers on the left and right are 667 and 238, respectively. The downstream location is 0.5" (x/d = 1.9). The images shown is 7 and 8 of the sequence, respectively.

In an effort to better understand the underlying reason of this mixing behavior, the stagnation chamber and pipe is rotated 90 degrees clockwise and additional data is collected. Again, sequenced data is presented in Figure 32 and Figure 33. The sampling rate is 6.5 Hz with an exposure time of 50 ms. The downstream location is 0.8 inches (x/d = 3.1). The data indicates that the jet orientation affects the behavior somewhat, although it is difficult to quantify. The concentration profile has slightly changed in shape, but the random motion outside of the core area remains indicative of helical mode jets.

Both helical and bifurcating jets are discussed in Chapter II. The jet behavior has more than one plume and in multiple directions. Jet plumes in bifurcating jets will extend further in the gravitational direction than observed and will only be observed in the gravitational direction. The jet is better described as five azimuthal fingers surrounding the core of the jet and is more characteristic of helical jets than bifurcating jets.

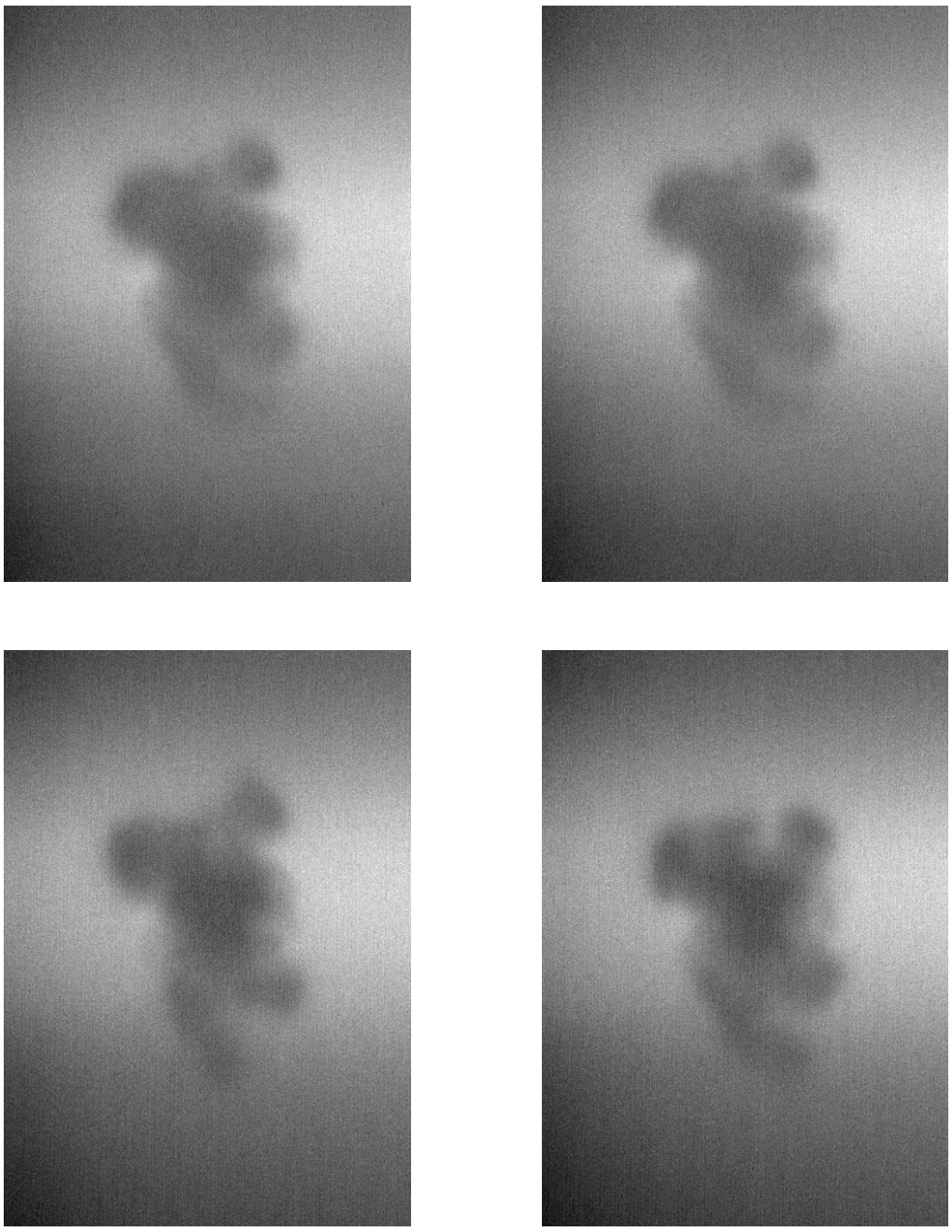

Figure 32. Sequenced data at a sampling rate of 6.5 Hz. The Reynolds numbers is 667 and the jet is rotated 90 degrees clockwise from the previous data set. The downstream location is 0.8" (x/d = 3.1). Sequence is from left to right, top to bottom. Images 1 – 4 of the sequence is shown.

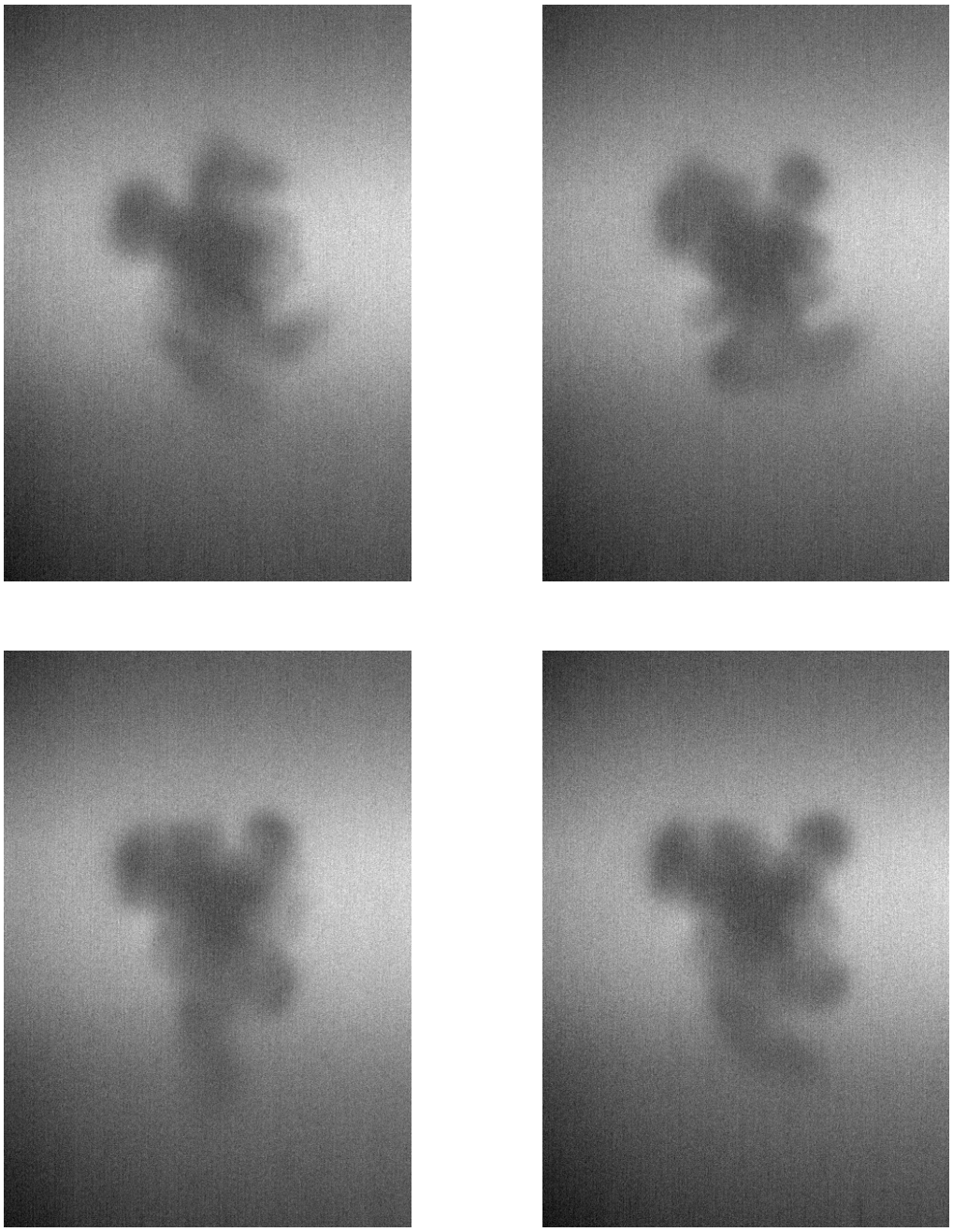

Figure 33. Sequenced data at a sampling rate of 6.5 Hz. The Reynolds numbers is 667 and the jet is rotated 90 degrees clockwise from the previous data set. The downstream location is 0.8" (x/d = 3.1). Sequence is from left to right, top to bottom. Images 5-8 of the sequence is shown.

Figure 34 displays mean helium concentration measurements and standard deviation data at a jet velocity of 41 ft/s, corresponding Reynolds number of 667, at a downstream distance of 0.8 inches (x/d = 1.9 to) with the jet rotated 90 degrees clockwise to further investigate the mixing characteristics. The core concentration measurements are approximately 0.93 and are comparable with the measurements calculated from the filtered top view data of the jet at 41 ft/s, ranging from 0.92 to 0.98 at x/d locations of 2.7 and 3.9, respectively. Figure 34 may be compared to Figure 25 and Figure 26. Qualitatively, it appears that some features of the jet do rotate 90 degrees but it is not a simple rotation.

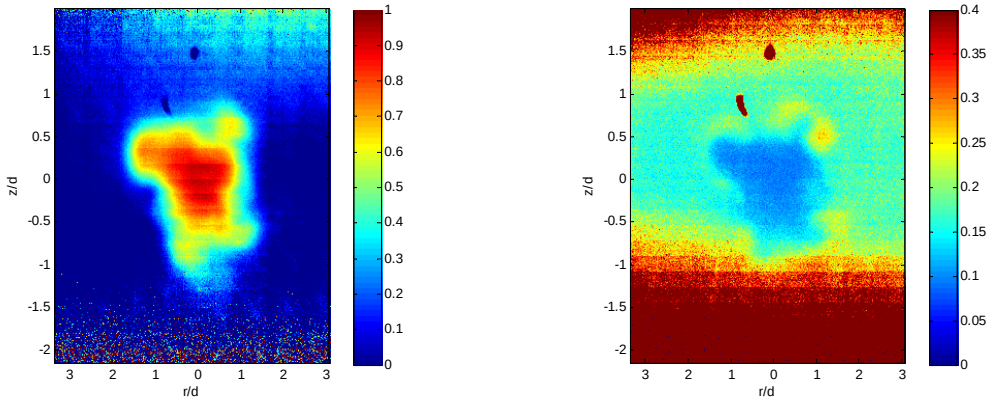

Figure 34. Time averaged helium concentration measurements and standard deviation of the jet oriented 90 deg clockwise from Figure 25. The downstream location is 0.8" (x/d = 3.1) and the jet velocity is 41ft/s.

Jet Trajectory

The jet trajectory is calculated by monitoring the z center position of the jet of the time averaged image. The z center position is chosen so that it is the average z value bounding helium concentration measurements of 70 percent at the center radial location. The jet trajectory for the collected data (x/d locations from 1.9 to 8.4) is shown in Figure 35. The flowfield conditions of the top graph have a Reynolds number of 667 and a Grashoff number of 1242. The flow conditions of the bottom graph in Figure 35 have a Reynolds number of 238 and a Grashof number of 1242. The referenced literature of Law et al, 2003, and Satyanarayana and Jaluria, 1982, predict and show a minimum trajectory for horizontal buoyant jets at the above conditions. The jet trajectory for the x/d location of 1.9 was calculated from their predictions. Their predictions were used to plot this trajectory position because no data was collected at an x/d location of zero. All other jet trajectory data is from the collected data. The jet regime is dominated by forced convection for both of the above conditions (White, 2006) and therefore a minimum jet trajectory is expected. A minimum jet trajectory is observed from the collected data as expected and is consistent with the literature (Law et al., 2003 and Satyanarayana and Jaluria, 1982).

A key advantage for using the time averaged image to calculate trajectory data is that the associated trajectory error becomes only a function of the user. One user might calculate the center of the jet at a pixel location of (X = 221,Y = 350), while another user might calculate the center of the jet at a pixel location of (X = 221, Y = 352). The error bars represent a +/- 4 pixel deviation between users.

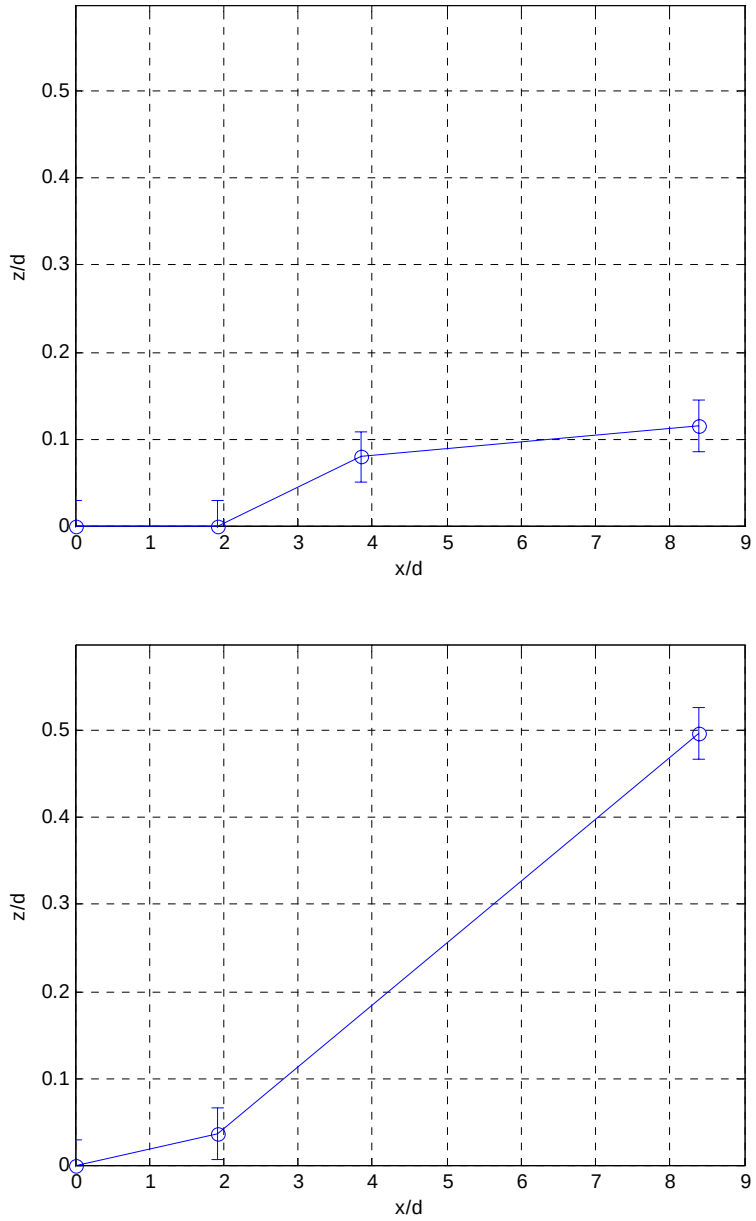

Figure 35. Forced convection dominates the jet regime and therefore the jet travels dominantly in the horizontal direction. The Reynolds number is 667 and 238 for the top and bottom graphs, respectively. The corresponding Grashof number is 1242.

Summary

The helium concentration measurements from the overhead and cross sectional view of the jet are in general agreement with one another. The behavior of the standard deviation plots is characteristic of jet mixing (Borg et al., 2001). The mixing behavior of the relatively high speed jet is indicative of a helical mode jet. The jet trajectory is characterized by the Reynolds and Froude numbers and the results correlate well with the literature, though the literature cited deals with larger x/d downstream locations.

V. Conclusions and Recommendations

Chapter Overview

The purpose of this chapter is to conclude the current research effort and make recommendations to future researchers in FRS. This research studies the data acquisition rate of FRS using a continuous argon ion laser with a PCO.4000 CCD and the behavior of a horizontal buoyant jet.

Investigative Questions Answered

A significant parameter of this research is the data acquisition rate of a FRS signal using a continuous argon ion laser and a PCO.4000 CCD. It is evident from Figure 12 that a FRS signal can be collected using a 10 ms exposure time. The camera manufacturer suggests a sampling rate of 80 Hz is attainable using the PCO.4000 camera. A 50 ms exposure time is chosen in this research due to its image clarity and relative ease of processing the data and is a stepping stone towards achieving an 80 Hz, or possibly even a 100 Hz signal, as the images collected at a 10 ms exposure time suggest is feasible.

The unfiltered and filtered helium concentration measurements are compared to study the effectiveness of the filter. The advantage for using a filter is clear. The filtered images have reduced noise to signal ratio levels compared to the unfiltered data. This is a direct result of the filter's capability to reduce the strength of unwanted reflections from walls and windows. The filter's effectiveness can be further maximized by appropriately characterizing the filter with the use of an interferometer.

Filtered Rayleigh scattering is a novel technique for flow diagnostics and is used to document the behavior of a horizontal buoyant jet in this research. Species concentration data is collected at different sampling rates to observe the jet behavior. The collected data are image files and the data processing involves analyzing the collected Rayleigh scattering signal.

Conclusions of Research

Typical FRS experiments use a pulsed laser and the data collection rate is limited to that of the laser, typically 10 -20 Hz. A PCO.4000 CCD can collect a FRS signal with a 10 ms exposure time as shown in Chapter IV. The data suggests a sampling rate of 80 Hz or even 100 Hz might be obtained, although this needs to be further investigated. Most of the data presented in this document was collected at 20 Hz.

The trajectory of the buoyant jet is consistent with the literature in that the Froude and Reynolds numbers are the governing parameters in determining the jet trajectory. However, mixing patterns for the buoyant jet indicate the core low-density fluid is expelled into the ambient region in a striking manner which suggests a form of helical mode excitation. The time averaged measurements reveal a five finger shaped pattern consistent with helical mode jets (Borg et al., 2001).

Significance of Research

The significance of this research is the investigation of collecting FRS data using a continuous argon ion laser. It would be formidable to collect a FRS signal at high frequencies. This research adds literature to the investigation of horizontal buoyant jets

and shows that the horizontal buoyant jet will become helical at certain operating conditions. As noted in Chapter I, there is a minute amount of literature on the horizontal buoyant jet versus the vertical buoyant jet.

Recommendations for Action

The sampling rate needs to be further investigated such that data can be collected at faster rates. This should be the primary focus of the next researcher. The effectiveness of the filter can be improved by characterizing it with the use of an interferometer and secondary power meter. Characterizing the filter in this way will provide invaluable insight as to selecting the best laser settings for FRS measurements and thus enhancing the collected signal at the shorter exposure times. Concentration data from the frontal view of the jet needs to be collected at more downstream locations, preferably coinciding with each downstream location collected from the overhead view, to fill out the trajectory data.

Recommendations for Future Research

Future research using the FRS system at AFIT should entail collecting velocity data in lieu of species concentration data. This should only be accomplished after the sampling rate is optimized and the filter is characterized as discussed in the previous section.

Summary

Species concentration measurements in a buoyant flowfield are collected using FRS. The mixing behavior of the jet is reveals a form of helical mode jets. The data

acquisition rate needs to be further investigated and the iodine absorption filter needs to be thoroughly characterized for future research.

Bibliography

Arakeri, Jaywant H., Das, Debopam and Srinivasan, J. (2000), "Bifurcation in a buoyant horizontal laminar jet," *Journal of Fluid Mechanics*, Vol. 412, pp. 61-73.

Bernard, Peter S. and Wallace, James M. Turbulent Flow Analysis, Measurement, and Prediction, John Wiley & Sons, 2002.

Boguszko, M. and Elliot, G.S. (2005), "Property measurement utilizing atomic/molecular filter-based diagnostics," *Progress in Aerospace Sciences*, Vol. 41, pp. 93-142.

Boguszko, M., Elliot, G. and Carter, C. (2002), "Filtered Rayleigh Scattering for Fluid/Thermal Systems," 22nd AIAA Aerodynamic Measurement Technology and Ground Testing Conference. June 24-27, 2002. St Louis, Missouri. AIAA Paper 2002-3233.

Boguszko, Martin and Elliot, Gregory S. (2004), "Measurements in Fluid Flows Using Molecular Filter-based Techniques," 42nd AIAA Aerospace Sciences Meeting and Exhibit. 5-8 January 2004. Reno, NV. AIAA Paper 2004-18.

Boguszko, Martin, Huffman, Rich and Elliot, Gregory S. (2006), "Property and velocity measurements in a supersonic flow," 44th AIAA Aerospace Sciences Meeting and Exhibit. 9-12 January 2006. Reno, NV. AIAA Paper 2006-1390.

Borg, A., Bolinder, J. and Fuchs, L. (2001),"Simultaneous velocity and concentration measurements in the near field of a turbulent low-pressure jet by digital particle image velocimetry-planar laser induced fluorescence," *Experiments in Fluids*, Vol. 31, pp. 140-152.

Chao, Y.-.C., Jong, Y.-C. and Sheu, H.-W. (2000), "Helical-mode excitation of lifted flames using piezoelectric actuators," *Experiments in Fluids*, Vol. 28, pp 11-20.

Hecht, Eugene. 4ed OPTICS, Addison Wesley, 2002.

Helmer, D.B. and Su, L.K. (2006), "Imaging of turbulent buoyant jet mixing," 44th AIAA Aerospace Sciences Meeting and Exhibit. 9-12 January 2006. Reno, NV. AIAA Paper 2006-309.

Helmer, D.B., Brownell, C.J. and Su, L.K. (2007),"Experimental investigations of mixing in turbulent jets with buoyancy," 45th AIAA Aerospace Sciences Meeting and Exhibit. 8-11 January 2007. Reno, NV. AIAA Paper 2007-1314.

Jiang, X. and Luo, K.H. (2003), "Dynamics and structure of transitional buoyant jet diffusion flames with side-wall effects," *Combustion and Flame*, Vol. 133, pp. 29-45.

Law, Adrian Wing-Keung, Wang, Hongwei, and Herlina (2003), "Combined Particle Image Velocimetry/Planar Laser Induced Fluoresence for Integral Modeling of Buoyant Jets," *Journal of Engineering Mechanics*, Vol. 129, pp. 1189-1196.

Lee, J., Won, S.H., Jin, S.H. and Chung, S.H. (2003), "Lifted flames in laminar jets of propane in coflow air," *Combustion and Flame*, Vol. 135, pp. 449-462.

McCartney, Earl J. Optics of the Atmosphere: Scattering by Molecules and Particles, John Wiley & Sons, 1976.

Miceli, David S. (2006), Characterizing a Co-flow Nozzle for use in a Filtered Rayleigh Scattering System, Master of Engineering thesis, Dept of Aeronautics, AFIT, WPAFB, OH.

Miles, R. and Lempert, W. (1990), "Flow diagnostics in unseeded air," 28th Aerospace Sciences Meeting. 8-11 January 1990. Reno, NV. AIAA Paper 1990-624.

Miles, Richard B., Yalin, Azer P., Tang, Zhen, Zaidi, Shoail H. and Forkey, Joseph N. (2001), "Flow field imaging through sharp-edged atomic and molecular 'notch' filters," *Institute of Physics Publishing. Measurement Science and Technology*, Vol. 12, pp. 442-451.

Miles, Richard B., Lempert, Walter R. and Forkey, Joseph N. (2001), "Laser Rayleigh Scattering," *Institute of Physics Publishing. Measurement Science and Technology*, Vol. 12, pp. R33-R51.

Miles, Richard B., Qian, Lipeng and Zaidi, Shoail H. (2006), "Imaging flow structure and species with atomic and molecular filters," *Optics and Lasers in Engineering*, Vol. 44, pp. 240-260.

Operator's Manual. The Coherent INNOVA Sabre-R Series Ion Laser. Coherent Inc, 2001.

Satti, Rajanii P. and Agrawal, Ajay K. (2006), "Computational Analysis of Gravitational Effects in Low-Density Gas Jets," *AIAA Journal*, Vol. 44, No. 7, pp. 1505-1515.

Satyanarayana, S. and Jaluria, Yogesh. (1982), "A Study of Laminar Buoyant Jets Discharged at an Inclination to the vertical Buoyancy Force," *Int. J. Heat and Mass Transfer*, Vol. 25, No. 10, pp. 1569-1577.

Seasholtz, Richard G. and Buggele, Alvin E. (1997), "Improvement in Suppression of Pulsed Nd: YAG Laser Light with Iodine Absorption Cells for Filtered Rayleigh Scattering Measurements," NASA Technical Memorandum 113177.

Shimizu, H., Lee, S.A. and She, C.Y. (1983), "High spectral resolution lidar system with atomic blocking filters for measuring atmospheric parameters," *Applied Optics*, Vol. 22, No. 9, pp. 1373-1381.

Sutton, Gavin, Levick, Andrew, Edwards, Gordon and Greenhalgh, Douglas (2006), "A combustion temperature and species standard for the calibration of laser diagnostic techniques," *Combustion and Flame*, Vol. 147, pp. 39-48.

White, Frank M. Viscous Fluid Flow, Third Edition, McGraw-Hill, 2006.

VITA

Christopher C. McGaha was born in Richmond, Virginia. In 2002, he earned a Bachelor of Science Degree in Mechanical Engineering from Virginia Polytechnic Institute and State University. Upon completion of his degree requirements, he was commissioned as a second lieutenant in the United States Air Force. He served as a Weapons Test System Manager from 2002 – 2005 and is currently a full time student at the Air Force Institute of Technology.

REPORT DOCUMENTATION PAGE

Form Approved
OMB No. 074-0188

1. REPORT DATE *(DD-MM-YYYY)*	**2. REPORT TYPE**	**3. DATES COVERED** *(From – To)*
15-03-2007	Master's Thesis	July 2006 – March 2007

4. TITLE AND SUBTITLE

FILTERED RAYLEIGH SCATTERING MEASUREMENTS IN A BUOYANT FLOWFIELD

5a. CONTRACT NUMBER
JON ENY 07-116

5b. GRANT NUMBER

5c. PROGRAM ELEMENT NUMBER

6. AUTHOR(S)

McGaha, Christopher C., Capt, USAF

5d. PROJECT NUMBER

5e. TASK NUMBER

5f. WORK UNIT NUMBER

7. PERFORMING ORGANIZATION NAMES(S) AND ADDRESS(S)
Air Force Institute of Technology
Graduate School of Engineering and Management (AFIT/EN)
2950 Hobson Way, Building 640
WPAFB OH 45433-8865

8. PERFORMING ORGANIZATION REPORT NUMBER
AFIT/GAE/ENY/07-M18

9. SPONSORING/MONITORING AGENCY NAME(S) AND ADDRESS(ES)
N/A

10. SPONSOR/MONITOR'S ACRONYM(S)

11. SPONSOR/MONITOR'S REPORT NUMBER(S)

12. DISTRIBUTION/AVAILABILITY STATEMENT
APPROVED FOR PUBLIC RELEASE; DISTRIBUTION UNLIMITED

13. SUPPLEMENTARY NOTES

14. ABSTRACT

Filtered Rayleigh Scattering (FRS) is a non-intrusive technique for studying flowfields. It utilizes a narrow linewidth laser, an absorption filter, and a detector. Molecular scattering provides the signal to the camera, and the difference in molecular cross section can be used to discriminate between unmixed gaseous components. The focus of this research is to document the behavior of a horizontal buoyant jet using FRS. A helium jet of precisely controlled mass flow rate is injected into a standard room temperature environment, and FRS provides the means to measure its core trajectory and mixing rate. Trajectory analysis, conducted with consideration of the Reynolds number and Grashof number, can be used to compare these results to the literature. A significant portion of the study was dedicated to measuring the rate at which FRS data can be acquired with a continuous wave laser. Additionally, mixing patterns for the buoyant jet were collected and indicate that core low-density fluid is expelled into the ambient region in a striking manner. Although such an expulsion of core low-density fluid has been noted in the literature, it has generally been associated only with an upward direction. This was observed at a Reynolds number of 238. However, at a Reynolds number of 667, the jet appears to take on features of jets subjected to an exaggerated form of helical mode excitation. The physics behind this phenomena requires additional study.

15. SUBJECT TERMS
Filtered Rayleigh scattering, Horizontal buoyant jet, Continuous laser

16. SECURITY CLASSIFICATION OF:Unclassified			**17. LIMITATION OF ABSTRACT**	**18. NUMBER OF PAGES**	**19a. NAME OF RESPONSIBLE PERSON**
a. REPORT	**b. ABSTRACT**	**c. THIS PAGE**			Reeder, Mark F., Professor, AFIT
U	**U**	**U**	**UU**	81	**19b. TELEPHONE NUMBER** *(Include area code)* (937) 255-3636, ext 4530 (mark.reeder@afit.edu)

Standard Form 298 (Rev. 8-98)
Prescribed by ANSI Std. Z39-18